A WEARABLE UNDERACTUATED KINESTHETIC DEVICE FOR INDUCING ARM SWING DURING GAIT REHABILITATION

by

Owen R. Barnes

A thesis submitted to the faculty of
The University of Utah
in partial fulfillment of the requirements for the degree of

Master of Science

Department of Mechanical Engineering

The University of Utah

May 2015

The University of Utah Graduate School

STATEMENT OF THESIS APPROVAL

The thesis of **Owen R. Barnes**

has been approved by the following supervisory committee members:

Jake J. Abbott	, Chair	**9/15/14** Date Approved
John M. Hollerbach	, Member	**9/24/14** Date Approved
Andrew S. Merryweather	, Member	**9/24/14** Date Approved

and by **Timothy A. Ameel**, Chair/Dean of

the Department/College/School of **Mechanical Engineering**

and by David B. Kieda, Dean of The Graduate School.

ABSTRACT

For those who have suffered stroke or spinal cord injury, rehabilitation is often the answer for improving gait function. Rehabilitative exercises, which often focus on the legs and deemphasize the role of the upper limbs, are done to help stimulate muscles and exploit neuroplasticity for the diminished functions. However, it has been shown that upper limb muscle activity can induce lower limb muscle activity. It has also been shown that proper arm swing is necessary during gait for balance.

This thesis presents the design concept and fabricated prototype of a device that swings the arms during gait rehabilitation. The device is low-powered, lightweight, wearable, and capable of assisting the user's arm swing in the sagittal plane and has unhindered kinematics in the remaining unactuated degrees of freedom. The design comprises three key subassemblies: a backpack frame, an underactuated arm-swing mechanism, and a power train to transfer and amplify motor torques to the arm-swing mechanism. Tests are performed to validate the shoulder-angle prediction equations based on the noncollocated motor-angle sensor measurements, to validate the device's ability to provide adequate torque to generate arm-swing in a passive user, and to investigate whether or not the user's active involvement can be observed by examining motor torque or shoulder angles. The results show that the device does provide sufficient torque to move the arms with a factor of safety, but that the model-based shoulder-angle estimates obtained from the motor measurements have nonnegligible error with the current prototype. It is recommended that a Proportional-Derivative (PD) controller with high PD gains be used with the device because of its low root mean square (RMS) tracking error, shoulder-angle amplitude creation, and ability to diagnose user-assistance level (i.e., is the user passive or actively assisting arm swing) online by observing shoulder-angle amplitudes and peak motor torques.

CONTENTS

LIST OF TABLES

ACKNOWLEDGMENTS

The road to completing this thesis has been a demanding one, and I would like to acknowledge and thank those who have helped me along the way. I would like to thank my advisor Jake Abbott for mentoring me these past years and for providing a critical eye that has only contributed to the success of this thesis. I would also like to thank Babak Hejrati for his assistance in developing and manufacturing this design as well as for his friendship. I would like to thank my labmates and friends Kyle Crandall and Sam Chesebrough for their help in the experiments. I would like to thank Michael Dale for his motivation and for helping me keep everything in perspective as I balanced my different responsibilities. Finally, I'd like to thank my parents, Randall and Claire Barnes, who have been a constant source of encouragement and motivation throughout all of my education and for supporting me in every decision I have made.

We acknowledge and are grateful to the National Science Foundation for supporting this project through the grant #1208637.

CHAPTER 1

INTRODUCTION

1.1 Motivation

Spinal cord injury (SCI) and stroke both affect the walking gait of those who suffer from it. As of 2013, there are an estimated 273,000 persons in the United States who suffer from SCI with 12,000 new cases each year [1]. Additionally, half of all SCI occur to young adults, from ages 16–30 years old. Strokes affect 795,000 people each year in the United States, around 610,000 of which are first attacks [2]. Strokes are the primary cause of long-term disability [2]. Clearly, these diseases affect many people's quality of living, oftentimes early in their life.

The walking gait of those who have had strokes or SCI is altered so that it is no longer healthy. Stroke patients often hold their affected upper limb to their side while their affected lower limb circumducts as they walk. With SCI, patients have difficulty moving their affected limbs because of their damaged motor and sensory neurons. In both cases, the patient needs to exert a great deal of physical and mental effort in order to walk. Thankfully, these people can undergo physical therapy in order to improve gait function. Rehabilitation is done through exercises that help stimulate muscles and exploit neuroplasticity for the diminished functions [3]. These exercises are most often accomplished with the aid of physical therapists. The therapists assist the patient through movements while encouraging the patient to use their muscles. Depending on the severity of the injury, these exercises can be labor intensive, requiring the therapists to carry out difficult manual tasks and/or requiring multiple therapists.

Gait rehabilitation is often focused on the legs and deemphasizes the role of the upper limbs. Studies show that there is neural coupling between the upper and lower limbs [4] and that it can be exploited for rehabilitative purposes [5]. Research also shows that upper limb muscle activity can actually induce lower limb muscle activity [6, 7] and that the effect is most pronounced when the arms move in phase with the legs [8]. Additionally, arm swing contributes balance to gait [4] and regulates rotational body motion [9] and metabolic

efficiency to the walker [10]. Therefore, more effective rehabilitation can be performed as the patient exerts effort to naturally swing their arms.

Currently, there exist several methods and technologies that assist with gait rehabilitation. One method of gait rehabilitation involving arm swing was shown in a study in which SCI subjects walked on a treadmill with their arms being manually assisted by a therapist with poles [4]. This type of rehabilitation allowed the subject to exercise both the upper and lower limbs. However, according to [11], rehabilitation is activity-dependent, and using devices (especially ones with upper-arm supports) can alter the input interpreted by the spinal cord, thus leading to the learning of incorrect muscle firing patterns. The poles support little weight, but that is dependent on the therapist's skill. It is important to allow the arms to swing as naturally as possible. Additionally, this method of rehabilitation requires several physical therapists to assist the patient during the exercise.

Many technologies have been developed for performing gait rehabilitation in an attempt to reduce the number of physical therapists required [12–16]. What these technologies have in common is that they are large, immobile, work-station type robotic orthoses. The devices precisely move the limbs through motions that help train the individual in walking functions. Two of the cited devices, the Lokomat [12] and the HapticWalker [16], have hand rests that—as previously mentioned—could encourage incorrect muscle learning in the arms if they are used. Some devices, like the LOPES [13] and the WalkTrainer [14], lack arm rests and allow the arms to be free. However, these devices provide no actuation for assisting arm swing. It is true that patients using the devices free of arm supports can swing their arms without any robotic assistance. Nevertheless, when the robot guides the legs through movements, the patient may have difficulty matching the pace and contralateral symmetry between the upper and lower limbs, thus missing the benefits that accompany moving the arms in phase with the legs [8]. One example of a robotic orthosis includes arm-swing assistance [15]. The robot consists of swinging prismatic links with handholds that interact with the subject's upper limbs, combined with sliding, height- and pitch-adjustable foot pads. Since the robotic system constrains the subject's feet and arms kinematically, it is likely that what the user experiences is dissimilar to natural, over-ground walking.

1.2 Conceptual Design

The previous section reviewed some of the current technologies available for gait rehabilitation. The devices successfully accomplish the task of training users by guiding their legs through repetitive motions. However, they do not properly assist, if at all, the arms so

as to exploit the neural coupling between the upper and lower limbs. This need for a device that properly swings the arms during the gait cycle for neurorehabilitative purposes has led to the development of the Underactuated WEarable Arm-swing Rehabilitator (UWEAR), shown in Figure 1.1. Instead of creating a large work-station robotic device, we have created a smaller, wearable, low-powered assistive device. The device is powered in just one degree of freedom (DOF) to assist in flexion/extension of the user's shoulder while allowing relatively free and uninhibited motion of the user's arms in the remaining DOF. The UWEAR is worn like a backpack on the user. Its arm links move in flexion/extension and abduction/adduction. The range of motion limits can be observed in Figure 1.2. The extension limit is restricted by the user's anatomical shoulder limits. The abduction limit is constrained by the travel length of the prismatic arm links. The flexion limit is determined by a combination of the sector-pulley arc length (located near the user's head) and the travel length of the prismatic arm link; one of these limits will occur before the other depending on the user's size. These ranges cover the motions necessary for both rehabilitation and relatively free movement while not performing rehabilitative tasks. Our goal was not to design a fully powered exoskeleton, but rather a device that assists the patient's arms in following a healthy gait at their own walking pace. The UWEAR (see Figure 1.3) comprises three key subassemblies: the All-purpose Lightweight Individual Carrying Equipment (ALICE) frame with additional supporting structures, underactuated

Figure 1.1. Demonstration of the UWEAR in arm-swing generation. The device is worn like a backpack, and provides active arm-swing assistance for flexion/extension of the shoulder, while being unconstraining in the other degrees of freedom.

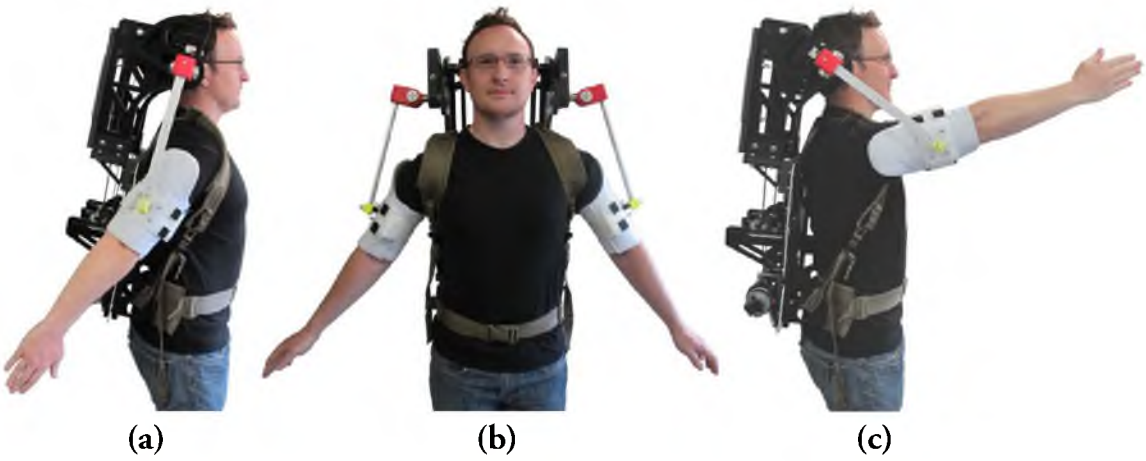

Figure 1.2. The user demonstrates the ranges of motion in the (a) extended, (b) abducted, and (c) flexed shoulder directions. The extension limit in (a) is constrained by the user's shoulder extension limits. The abduction limit in (b) is determined by the travel length of the prismatic arm links. The flexion direction in (c) is limited by a combination of the sector-pulley arc length and prismatic arm link depending on the size of the user.

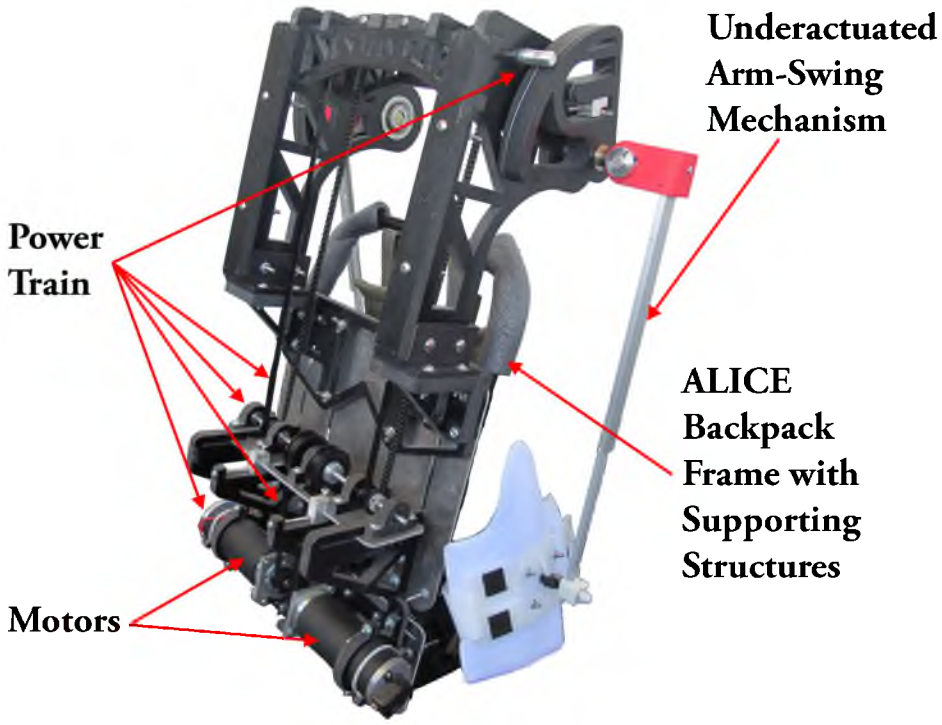

Figure 1.3. The Underactuated WEarable Arm-swing Rehabilitator (UWEAR) is composed of several subassemblies: the ALICE backpack frame with additional supporting structures, an underactuated arm-swing mechanism, and a power train to convert motor torque to torque for the arm-swing mechanism.

arm-swing mechanisms to generate arm swing in shoulder flexion/extension while allowing unconstrained motion in remaining DOF, and a power train to convert torque generated by DC motors located near the user's hips to amplified torque for the arm-swing mechanisms.

The underactuated arm-swing mechanism applies power to the user's arms from the power train in the "arm-swing" direction without constraining the arms in the other unactuated DOF. The assemblies are located lateral to the user's arms. They start above the user's shoulders, near the user's head, from the UWEAR's supporting structures, and extend to the user's arms via arm cuffs. The assemblies comprise five joints each, all with one DOF. Only the shoulder flexion/extension DOF is actuated in the assemblies.

A military All-purpose Lightweight Individual Carrying Equipment (ALICE) backpack frame provides both a foundation for the rest of the mechanism and a secure fit on the user. The ALICE frame is made of aluminum and steel. The strength and rigidity of the metals along with the adjustable shoulder and waist straps accomplish two objectives. They provide adequate reaction forces to ensure that power is spent in moving the arms, rather than moving the frame relative to the user's body. Additionally, the strength and rigidity of the frame prevent the structure from flexing from the torques caused by the motors.

Additional structural components support the underactuated arm-swing mechanism and power train so that power is spent only in moving the user's arms and not in the flexing the structure. Acrylonitrile butadiene styrene (ABS) plastic is chosen for its strength and weight. Screws fasten two slotted aluminum plates to the ALICE frame. The slots allow for positioning the device's components and allow for modular additions (e.g., the power train's tensioning shelf and motor mounts). Several bolts and slots in the structural components provide adjustability for the UWEAR so that it fits a large population.

The power train—comprising motors, a timing-belt system, and capstan drives—is located on the back of the ALICE frame. The timing-belt system transfers torque from the motors, which sit by the user's hips, up to the input to the underactuated arm-swing mechanism, which is located above the user's shoulders. The timing-belt assembly has stages of pulleys that amplify the motor torques. After the first stage of pulleys there is a tensioning device, and by adjusting its positioning screws, it can eliminate slack in the timing-belts. Large direct-drive motors (i.e., no gearhead) provide relatively high torque while being backdrivable. The power train's final stage is the capstan drive, which further amplifies the motor torque while maintaining the backdrivability of the power train.

1.3 Thesis Outline

The remainder of this thesis is structured as follows. Chapter 2 discusses the relevant kinematics and dynamics of the human arm; it gives an understanding of the expected range of motion and torques required for arm swing. Chapter 3 presents the design concept of the underactuated arm-swing mechanism. Chapter 4 presents the design concept of the power-train assembly, which provides the torque to the underactuated arm-swing mechanism. Chapter 5 combines the results of Chapters 2–4 to synthesize the design of a prototype device. Chapter 6 describes experiments that are used to validate the prototype device. Finally, Chapter 7 provides conclusions and recommendations for future work.

CHAPTER 2

THE HUMAN ARM

The kinematics and dynamics of the human arm are important factors in the design of the UWEAR. The kinematics of the shoulder are important to determine how to generate torque for arm swing while not overly constraining the user. The dynamics of the arm give an idea of the required torques needed to assist the user during rehabilitation and provide specifications for the design of a successful device.

2.1 Kinematics of the Shoulder

The shoulder is a complex feature with several degrees of freedom. Its two joints of interest include the glenohumeral (GH) and scapulothoracic (ST) joints. The GH joint is a ball-and-socket joint formed by the head of the humerus and the glenoid cavity of the scapula. This joint allows for motions in three rotational degrees: flexion/extension, abduction/adduction, and medial/lateral rotation. The ST joint is a pseudojoint between the anterior surface of the scapula and the posterior thoracic side of the rib cage. This joint has five DOF; two are translational and three are rotational. The translational movements are protraction/retraction and elevation/depression. The rotational movements include upward/downward rotation, anterior/posterior tilt, and external/internal rotation about a cephalo-caudal (i.e., longitudinal) axis [17]. This last DOF is often referred to as "scapular winging."

It is the goal of our design to assist only the flexion/extension of the GH joint. The other motions of the GH and ST joints are to remain uninhibited. The abduction/adduction DOF of the GH joint is especially desired since the upper limb, as it sagittally rotates, does not follow a straight line when viewed in the transverse plane. There is one DOF that is the exception to our desired to remain uninhibited: medial/lateral rotation of the GH joint; it is later found that this DOF complicates the control of the arm with our concept design, and we must therefore limit its motion. Kinematic information of the shoulder is important in the UWEAR's design. Its influence on the mechanism's design is discussed in Chapter 3.

2.2 Dynamic Model of the Human Arm

The upper arm and forearm of the human user can be mathematically modeled as a two-link pendulum. The free-body diagram, as seen in Figure 2.1, includes torques stemming from inertia, gravity, coriolis, stiffness, damping, and elbow lock (i.e., the mechanical stop that prevents the elbow from hyper-extending). These sum to give an estimate of the shoulder and elbow torques. The arm lengths are represented by a_i, where the subscript i signifies the i-th arm link, where $i = 1$ and $i = 2$ represent the upper arm and forearm, respectively. The joint angels are represented by θ_i, where $i = 1$ and $i = 2$ represent the shoulder and elbow angles, respectively. The distance from the joint to the center of gravity is called l_i. The mass of each arm link is represented by m_i. The rotational inertia of each link is calculated about its center of gravity and is denoted by I_i. The acceleration of gravity is represented by g. The matrix $\mathbb{H}$ includes the inertial terms, $\mathbb{V}$ contains the centripetal and coriolis terms, $\mathbb{G}$ contains the gravity terms, $\mathbb{N}$ has the joint stiffness and viscous damping terms, and $\vec{\tau}_{lock}$ has the torque from elbow lock. Prior work [18] provides reasonable values for the entries found in $\mathbb{N}$ and $\vec{\tau}_{lock}$. The final mathematical model describing the dynamics of the arm is

$$\vec{\tau}_{arm} = \begin{bmatrix} \tau_{sh} \\ \tau_{elb} \end{bmatrix} = \mathbb{H} \begin{bmatrix} \ddot{\theta}_1 & \ddot{\theta}_2 \end{bmatrix}^T + \mathbb{V} \begin{bmatrix} \dot{\theta}_1^2 & \dot{\theta}_1\dot{\theta}_2 & \dot{\theta}_2^2 \end{bmatrix}^T + \mathbb{G} + \mathbb{N} + \vec{\tau}_{lock} \tag{2.1}$$

where $\mathbb{H}$, $\mathbb{V}$, $\mathbb{G}$, $\mathbb{N}$, and $\vec{\tau}_{lock}$ are defined as follows:

$$\mathbb{H} = \begin{bmatrix} m_1 l_1^2 + m_2(a_1^2 + l_2^2 + 2a_1 l_2 \cos\theta_2) + I_1 + I_2 & m_2(l_2^2 + a_1 l_2 \cos\theta_2) + I_2 \\ m_2(l_2^2 + a_1 l_2 \cos\theta_2) + I_2 & m_2 l_2^2 + I_2 \end{bmatrix} \tag{2.2}$$

$$\mathbb{V} = \begin{bmatrix} 0 & -2m_2 a_1 l_2 \sin\theta_2 & -m_2 a_1 l_2 \sin\theta_2 \\ 2m_2 a_1 l_2 \sin\theta_2 & 0 & 0 \end{bmatrix} \tag{2.3}$$

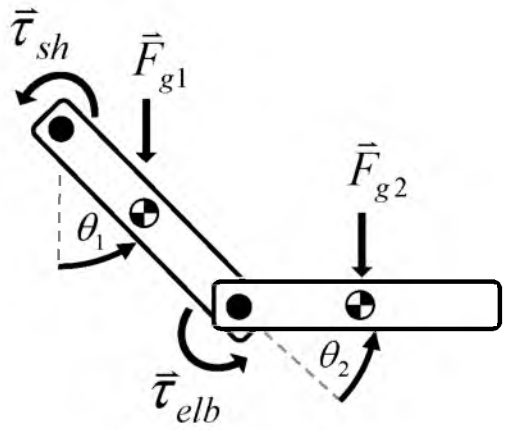

Figure 2.1. The upper and lower arm are modeled as a double pendulum. Inertial, gravity, coriolis, stiffness, damping, and elbow-lock torque sum to give an estimate of the shoulder and elbow torques.

$$\mathbb{G} = \begin{bmatrix} g(m_1 l_1 \sin\theta_1 + m_2(l_2 \sin(\theta_1+\theta_2) + a_1 \sin\theta_1)) \\ g(m_2 l_2 \sin(\theta_1+\theta_2)) \end{bmatrix} \tag{2.4}$$

$$\mathbb{N} = \begin{bmatrix} 0.9\theta_1 + 0.1\dot{\theta}_1 \\ 0.9\theta_2 + 0.1\dot{\theta}_2 \end{bmatrix} \tag{2.5}$$

$$\vec{\tau}_{lock} = \begin{bmatrix} 0 \\ 0.5e^{-7\theta_2} \end{bmatrix} \tag{2.6}$$

Although we would typically think of the joint torques as the input to the system and the joint motion as the resulting output, this model can be used in an inverse-dynamics fashion to determine the joint torques required to generate a given arm trajectory. In order to obtain joint-torque estimates with this model, the joint trajectories first need to be characterized.

2.3 Estimating Joint Torques from Arm-Swing Trajectories

Realistic joint trajectories are required for an accurate estimate of the joint torques. Joint trajectories are created here based on the trajectory features (i.e., amplitude, mean offset, phase, and frequency) found in [19]. According to that study, the shoulder joint trajectory can be characterized by a signal centered at -10 degrees with an amplitude of 20 degrees. The elbow is defined by a signal centered at 5 degrees with an amplitude of 5 degrees. There is no phase difference between the two signals, so the joints are fully flexed and extended at the same instants in the cycle. The two joints have the same frequency, which is the person's stepping frequency. The trajectories in [19] are not purely sinusoidal, but for simplicity in designing the UWEAR, we assume them to be. The amplitudes and phases of the extrema for the joints angles are the most important parameters for estimating the maximum torque.

Figure 2.2 shows the joint-angle and torque trajectories that are produced from the mathematical model of the human arm by using inverse dynamics. The mass and length of the arms are determined from proportions derived by [20] and [21]. The height and mass of the user is assumed to be 1.9 m and 100 kg, which represents a large human for a maximum-torque-requirement scenario for our design, resulting in $m_1 = 2.63$ kg, $m_2 = 1.61$ kg, $a_1 = 0.35$ m, and $a_2 = 0.28$ m. The torque trajectory is examined to estimate the required shoulder torques. Upon inspection, it is found that the maximum torque of 4.3 N·m at the arm's fully flexed position—at 10 degrees—is required for the desired motions. This torque magnitude is reasonable when compared with the results from prior studies [9], [10], [22], [23], which report torques in the range of 2.2–12 N·m. The derived torque requirements serve as a reference point that guides the design decisions that are discussed later in Chapter 5.

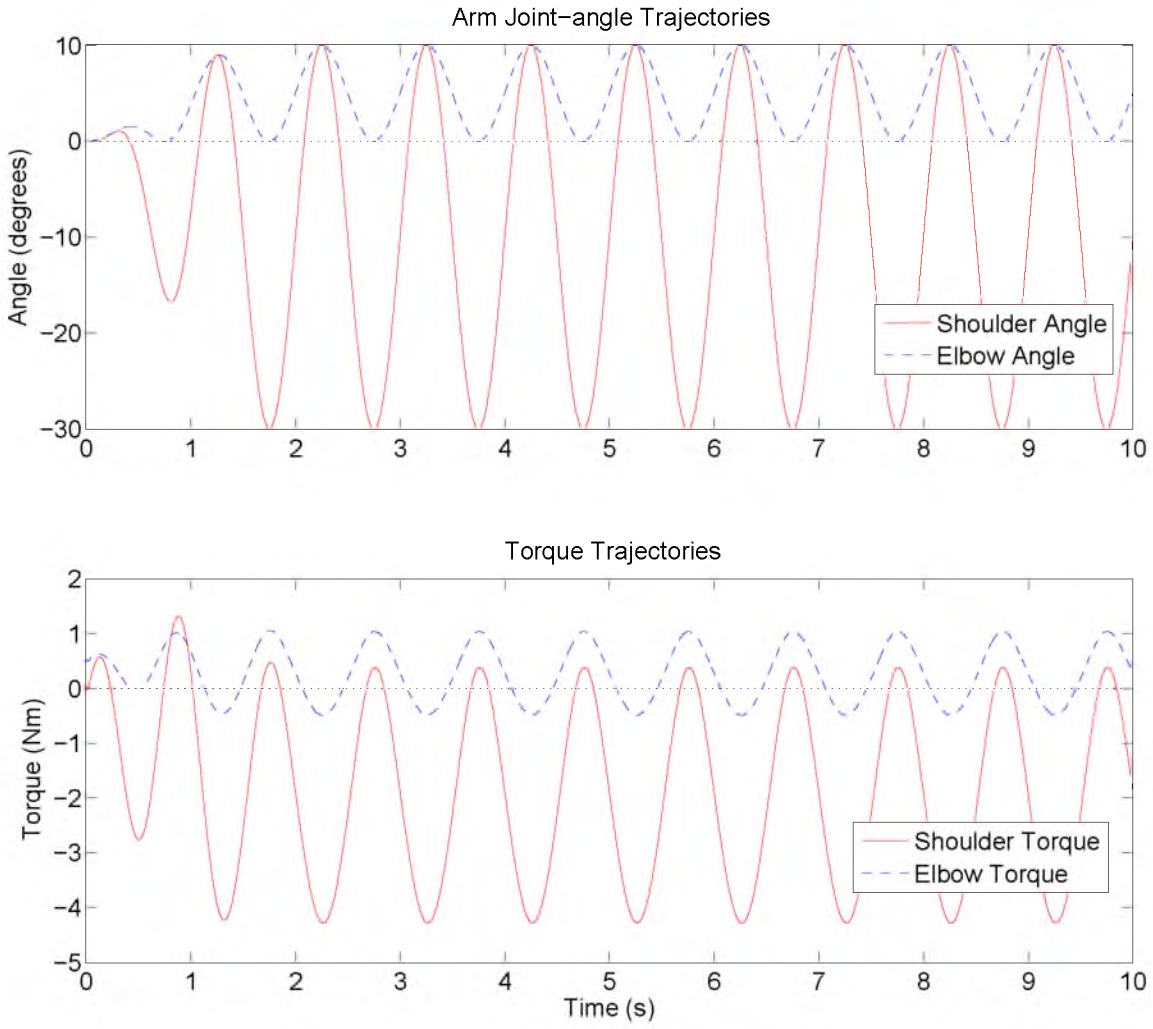

Figure 2.2. Joint-angle trajectories and the joint torques required to produce them for arm swing at a frequency of 1.0 Hz for a 1.9-m-tall and 100-kg person. The torque plot indicates that the UWEAR needs to create a shoulder torque of 4.3 N·m in order to generate arm swing at this frequency. This figure also shows that the maximum torque expected occurs at the extremes of the arm-swing trajectory, with the largest torque occurring at the shoulder's fully flexed position.

CHAPTER 3

UNDERACTUATED ARM-SWING MECHANISM

In this chapter, the components of the underactuated arm-swing mechanism are described in greater detail. Figure 3.1 shows a close-up of the key components of the mechanism. It shows the torque input, which receives torque from a torque-generating device like a motor or hydraulic system. In our prototype, the torque input is generated by the power train described in Chapter 4, but in this chapter we abstract the torque input and focus on the design of the arm-swing mechanism. The input lies above and behind the user's shoulder. The torque input drives the first degree-of-fredom (DOF) of the 2-DOF shoulder joint in flexion/extension. The second DOF in the 2-DOF shoulder joint is passive and allows for abduction/adduction of the user's arm. The prismatic link, a passive joint that allows for unhindered motions, transmits the torque from the 2-DOF shoulder joint to the 2-DOF cuff joint. The cuff joint allows for angular deviations between the user's arm and the prismatic link in both flexion/extension and abduction/adduction. The arm

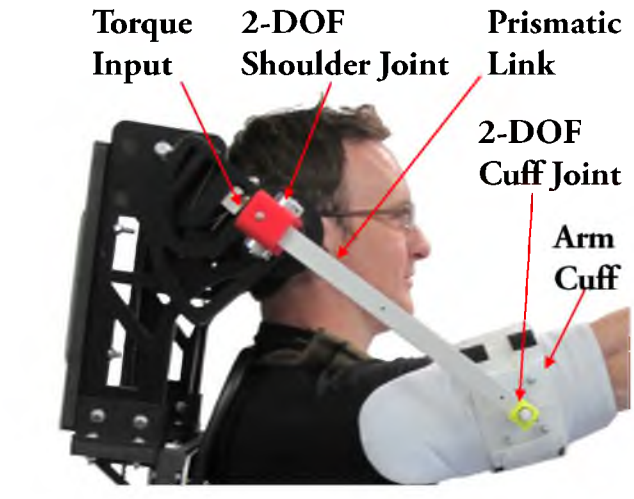

Figure 3.1. A close-up of the underactuated arm-swing mechanism showing its key components.

cuff permits forces to be transferred from the mechanism to the user's arm. This force creates an equivalent motion to move the arm in flexion/extension to what would normally be generated by the user's shoulder. Section 3.1 discusses these and other components in greater detail, and Section 3.2 discusses the kinematics of the powered DOF and the resulting arm-swing.

3.1 Development of the Underactuated Arm-Swing Mechanism

3.1.1 Shoulder Joint

Figure 3.2 shows the arm-swing mechanism's shoulder joint comprised of two 1-DOF components. It allows the mechanism to assist in flexion/extension of the glenohumeral joint using torque from the torque input. The assembly also allows the user to abduct/adduct the arm. The joint is made of a bearing that sits in a neighboring structural part. The bearing contains a spacer that holds a clevis within it. This clevis extends away from the user and interfaces with a pin with two attached bearings. These two bearings are housed in a 3D printed part. The joint between the clevis and the 3D printed part is passive and allows the user to abduct/adduct the upper arm. The 3D printed part hugs the outsides of the clevis with two prongs, rather than using one prong to interface with the inside faces of the clevis, to better allow the part to bear the stresses from arm swing.

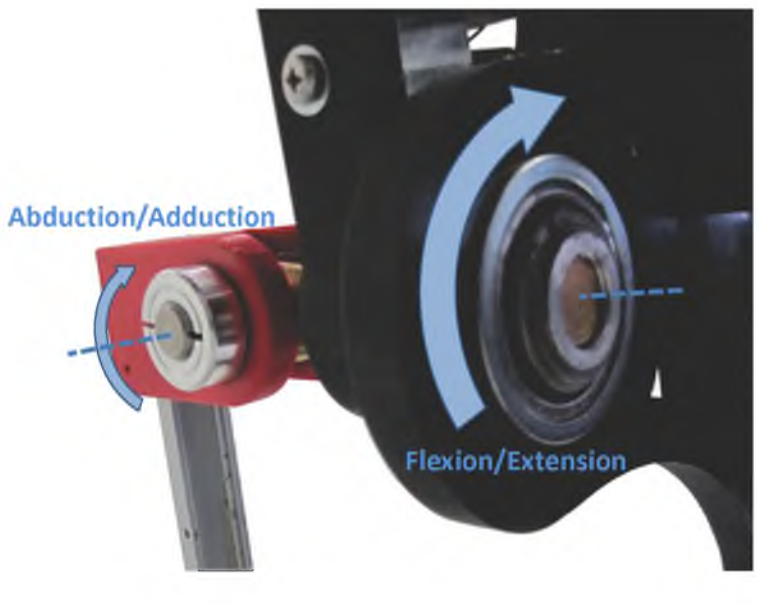

Figure 3.2. The shoulder joint comprises two 1-DOF joints, which allow for flexion/extension and abduction/adduction movements of the user's arm. The flexion/extension DOF is the only powered DOF in the arm-swing mechanism.

3.1.2 Prismatic Arm Link

The prismatic arm link is used in concert with the 2-DOF shoulder joint for assisting the user's arm in flexion/extension while accounting for the necessary change in link length during both flexion/extension and abduction/adduction. A length-varying link is necessary since the device's shoulder axis and the user's shoulder axis are not coincident. Even if the axes were designed to be nominally coincident, there would still be a need for a length-varying link since the user's shoulder position can change from scapulothoracic motions. A solid link would resist the changing positions of the user's shoulder, resulting in a feeling of binding. Additionally, a prismatic link allows for free abduction/adduction that comes from the changing mediolateral distance between the user's arm and torso due to arm swing not following a straight line as viewed in the transverse plane, and it accounts for different nominal lengths for this link for users of different size. In order to account for this changing length, the prismatic link contains telescopic slide rails. The slide rails house bearings that make its length adjustments smooth and with little friction.

3.1.3 Cuff Joint

A small assembly connects the prismatic arm link and the upper arm. It includes the distal 3D-printed bearing housing, the eyelet and clevis rod end, and the arm cuff. Together the components comprise the 2-DOF cuff joint.

The first component of interest is the small 3D-printed part placed at the distal end of the telescopic slide rails. The part houses bearings and a threaded eyelet. The assembly is held together with jam nuts (as shown in Figure 3.3). This revolute joint allows for the relative

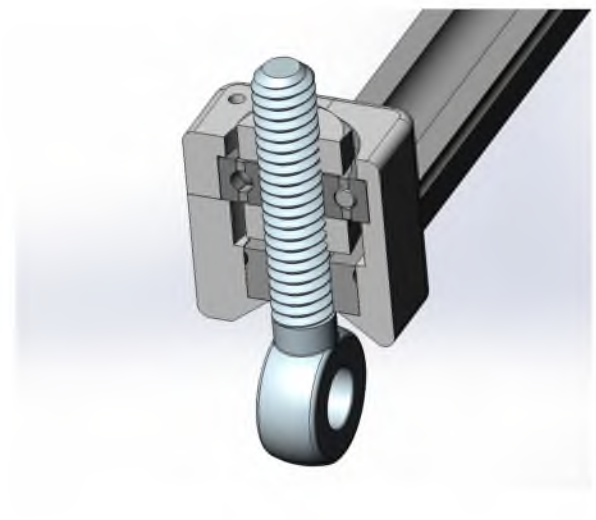

Figure 3.3. CAD model showing the cross-section of the distal bearing housing. The eyelet rotates with the bearing and is held in place by jam nuts.

rotation between the prismatic arm link and the upper arm as the user flexes/extends the arm. The jam nuts mate with the threaded eyelet and are placed on both sides of the bearing to immobilize the threaded eyelet in the housing. Keeping the threaded eyelet in place minimizes the moment arm created by it and the adjacent clevis rod end. The reduction of this moment arm lessens the undesired torque that causes internal/external rotation of the upper arm.

To permit unhindered movement, the threaded eyelet mates with a clevis rod end. It allows for the abduction/adduction of the user's upper arm. Again, the need for this originates from the offset between the shoulder axes of the user and mechanism. As the user abducts/adducts the arm, the prismatic arm link adjusts its length so it can follow the circular path traced out by the arm cuff. The revolute joint formed by the eyelet and clevis rod end allows for angular differences between the arm link and upper arm during abduction/adduction. The clevis rod end sits in the arm cuff as seen in Figure 3.4. Sheet plastic prevents rotation of the clevis rod end about an axis normal to the arm cuff's surface. It keeps it in place by passing through the yoke formed by the clevis. Without this motion restriction for the clevis rod end, the clevis rod end's abduction/adduction axis would be able to change orientation, creating awkward and uncontrollable pulling motions.

The arm cuff is worn on the user's upper arm. It is responsible for remaining stationary to increase the effectiveness of the forces transmitted to the arm from the mechanism. It has an elastic band that helps the arm cuff remain tight on the upper arm. To assist the elastic's purpose, some sheet plastic is added with hook-and-loop (shown in Figure 3.5), adding more stability to the arm cuff. The better the arm cuff can resist internal/external rotation on the upper arm, the better it can transmit forces to generate arm swing. Moreover, the

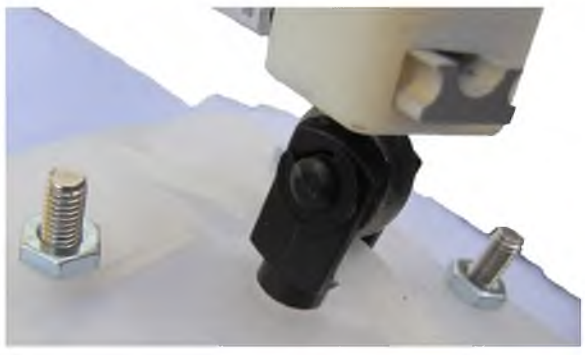

Figure 3.4. The threaded eyelet and clevis rod end add a DOF vital for permitting uninhibited abduction/adduction of the user's arm. Also shown is the sheet plastic that passes through the clevis. This is important for limiting the unwanted DOF.

Figure 3.5. The arm cuff provides a secure attachment point to the user. The cuff, along with the sheet plastic and hook-and-loop, resist forces and slipping. This ensures good force transmission.

arm cuff keeps the prismatic arm link in phase with the upper arm (i.e., it prevents the prismatic arm link from leading or lagging the arm), which keeps force transmission smooth, predictable, and controllable. The arm cuff's hook-and-loop also prevents it from sliding up and down the user's arm. This discourages the cuff from drifting toward the user's elbow joint, which can limit the joint's range of motion.

3.2 Kinematics of the Powered Degree of Freedom

The purpose of the underactuated arm-swing mechanism is to assist the user's arm in glenohumeral flexion/extension while allowing for uninhibited movement in the shoulder's other DOF. The previous section described the design choices to provide basic functionality. In this section, we find the actual kinematic equations that govern the mechanism in the single DOF associated with arm swing. In Figure 3.6, the basic geometry describing the mechanism in two different configurations is illustrated. The geometry includes

- O_s, the user's shoulder axis
- O_m, the arm-swing mechanism's powered axis
- b, the vertical offset between the two axes
- a, the horizontal offset between the two axes
- θ_s, the relative angle of the upper arm
- θ_m, the relative angle of the prismatic link
- O_c, the connection point between the mechanism and the user's upper arm
- R, the distance between the user's shoulder axis and connection point
- $L(\theta_s)$, the length of the mechanism's prismatic link, which is a function of θ_s

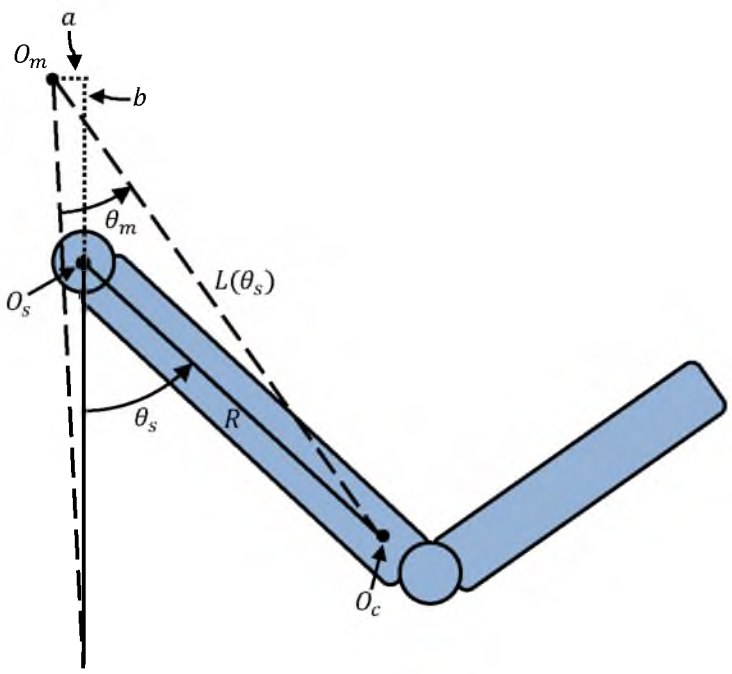

Figure 3.6. Basic geometric layout of the arm-swing mechanism, shown in two different configurations: vertical (0 degrees) and flexed. The user's arm is depicted in the flexed position to show how it relates to the layout geometry.

The offsets a and b are included since it is unrealistic to place the arm-swing mechanism's powered axis to always coincide with the user's shoulder axis. Rigidly placing the mechanism's powered axis over the user's shoulder axis ignores the changing position of the shoulder (i.e., glenohumeral) joint due to scapulothoracic movements and invites the possibility of hindering the scapulothoracic motions. In addition to accounting for scapulothoracic movements, the basic geometry chosen allows for flexion/extension and abduction/adduction of the glenohumeral joint, as well as a "one size fits all" design.

The relationship between the user's shoulder angle, θ_s, and the arm-swing mechanism's prismatic-link angle, θ_m, are important for the design and control of the device. The relationship can be used to estimate the user's shoulder angle (unsensed) from the θ_m (sensed), and it can also be used to convert a desired user shoulder angle into a desired mechanism angle. First, we must attribute some additional parameters to our geometry, as shown in Figure 3.7. The parameter L_0 is the length of the prismatic link in the "zero" position, when $\theta_s = 0$. D, which represents the offset between the axis of the user's shoulder and the powered axis of the mechanism, is simply the hypotenuse of the right triangle whose legs are formed by a and b:

$$D = \sqrt{a^2 + b^2} \tag{3.1}$$

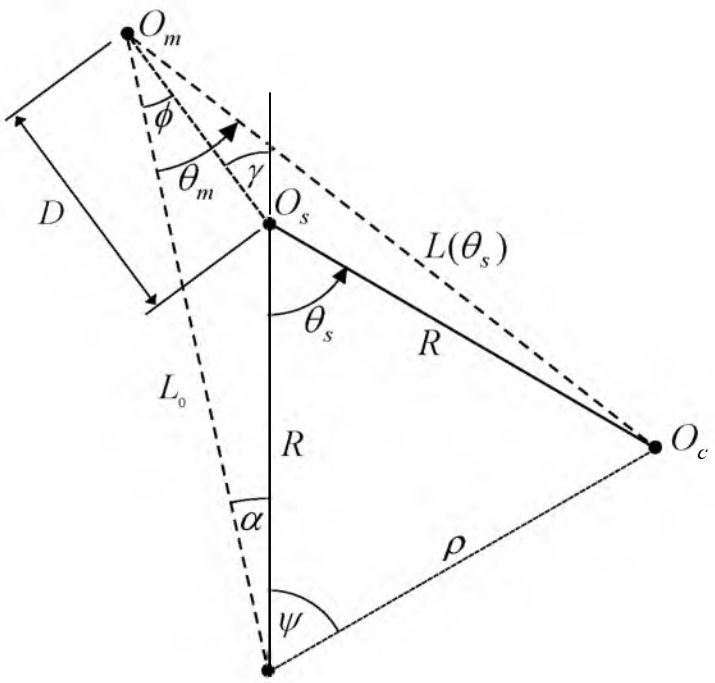

Figure 3.7. Geometry of the powered DOF of the arm-swing mechanism, shown in two different configurations: with the upper arm vertical, which we refer to as the "zero" position, and with the upper arm flexed to an arbitrary shoulder angle. The parameters that are used for calculating the relationship between the arm-swing mechanism and the user's shoulder angle are shown.

The angle γ represents the angle between D and the vertical. The angle α describes the angle between the user's upper arm and the prismatic link in the "zero" position. The angle ϕ represents the angle between D and L_0. A number of additional useful relationships follow:

$$\alpha = \arctan\left(\frac{D\sin\gamma}{D\cos\gamma + R}\right) \tag{3.2}$$

$$\phi = \gamma - \alpha \tag{3.3}$$

$$L_0 = \frac{R\sin(\pi - \gamma)}{\sin\phi} \tag{3.4}$$

It is now possible to find the relationship between the shoulder angle and the mechanism angle. First, the length of the prismatic link is calculated as

$$L = D\cos(\theta_m - \phi) + \sqrt{R^2 - D^2\sin^2(\theta_m - \phi)} \tag{3.5}$$

The Law of Cosines can then be used to find the cosine of the user's shoulder angle:

$$\cos(\theta_s) = 1 - \frac{L^2 + L_0^2 - 2LL_0\cos(\theta_m)}{2R^2} \tag{3.6}$$

Equation 3.6 is rearranged to a more numerically robust form using a trigonometric half-angle formula involving the tangent and cosine of the same angle:

$$\theta_s = \pm 2 \arctan \sqrt{\frac{1 - \cos(\theta_s)}{1 + \cos(\theta_s)}} \tag{3.7}$$

Substituting the solutions for $\cos(\theta_s)$ from (3.6) into (3.7) gives the final relationship between the arm-swing mechanism's angle and the user's shoulder angle:

$$\theta_s = \pm 2 \arctan \sqrt{\frac{L^2 + L_0^2 - 2LL_0 \cos(\theta_m)}{4R^2 - L^2 - L_0^2 + 2LL_0 \cos(\theta_m)}} \tag{3.8}$$

The positive solution for θ_s is used when θ_m is positive, the negative solution is used when θ_m is negative, and when θ_m is zero, θ_s is also zero.

The geometric model here assumes that the shoulder joint is a static pin joint. However, the shoulder joint is capable of moving due to its scapulothoracic degrees of freedom. Therefore, (3.8) is not a relationship that will predict the shoulder angle with high accuracy, but rather it will approximate it. This result is seen in the experiments done in Chapter 6.

CHAPTER 4

POWER TRAIN, ALICE FRAME, AND SUPPORTING STRUCTURES

In the previous chapter, it was assumed that torque was being generated as an input to the arm-swing mechanism, but with no discussion of how that torque would be generated. This chapter discusses the concepts of the power train, which is our solution for providing torque to the arm-swing mechanism. The term "power train" is used to include all elements of the UWEAR that deal with transmitting motor torque to the torque required by the arm-swing mechanism. It includes the motors, timing-belt system, and capstan drive. Additionally, the concept of the ALICE frame and other supporting structures, which bear the components of the power train and the underactuated arm-swing mechanism, are discussed.

4.1 Power Train

4.1.1 Motors

DC motors are chosen as the principal actuation source for the UWEAR. The motors are fastened on the back side of the ALICE frame near the user's hips. The location and spatial size of the motors are such that they do not obstruct the user's arms as they swing them during walking nor do the motors interfere with each other. The motors provide torques for assisting the movement of the user's arm in flexion/extension. The motors are direct drive and backdrivable; they do not have an attached gearbox, which would add friction and inertia to the power train. Motor backdrivability allows the whole UWEAR device to be unconstraining on the user's motions while unpowered, which is desirable for fail-safe operation and easy donning/doffing of the device.

4.1.2 Timing-Belt System

The limited torque provided by relatively small motors calls for a torque multiplying element. A timing-belt system is chosen to accomplish this task. The timing-belt system

allows the entire transmission to remain backdrivable, backlash free, and be made of lightweight components. The subassembly is composed of two stages of timing pulleys and belts for each arm. The pairs of timing belts meet at what is referred to as the tensioning shelf. The timing-belt assembly is located on the back of the UWEAR on the ALICE frame. The belts span the distance from the motor shaft, which is located near the user's hips, to the torque output shaft, which is located above and behind the user's head.

The timing-belt system can be seen in Figure 4.1. The two sets of timing pulleys provide two stages of torque amplification. The gear ratio, k_{TB}, for the timing-belt system is described by

$$k_{TB} = \frac{d_2 d_4}{d_1 d_3} \tag{4.1}$$

where the parameters d_1, d_2, d_3, and d_4 represent the pitch diameters of the timing pulleys,

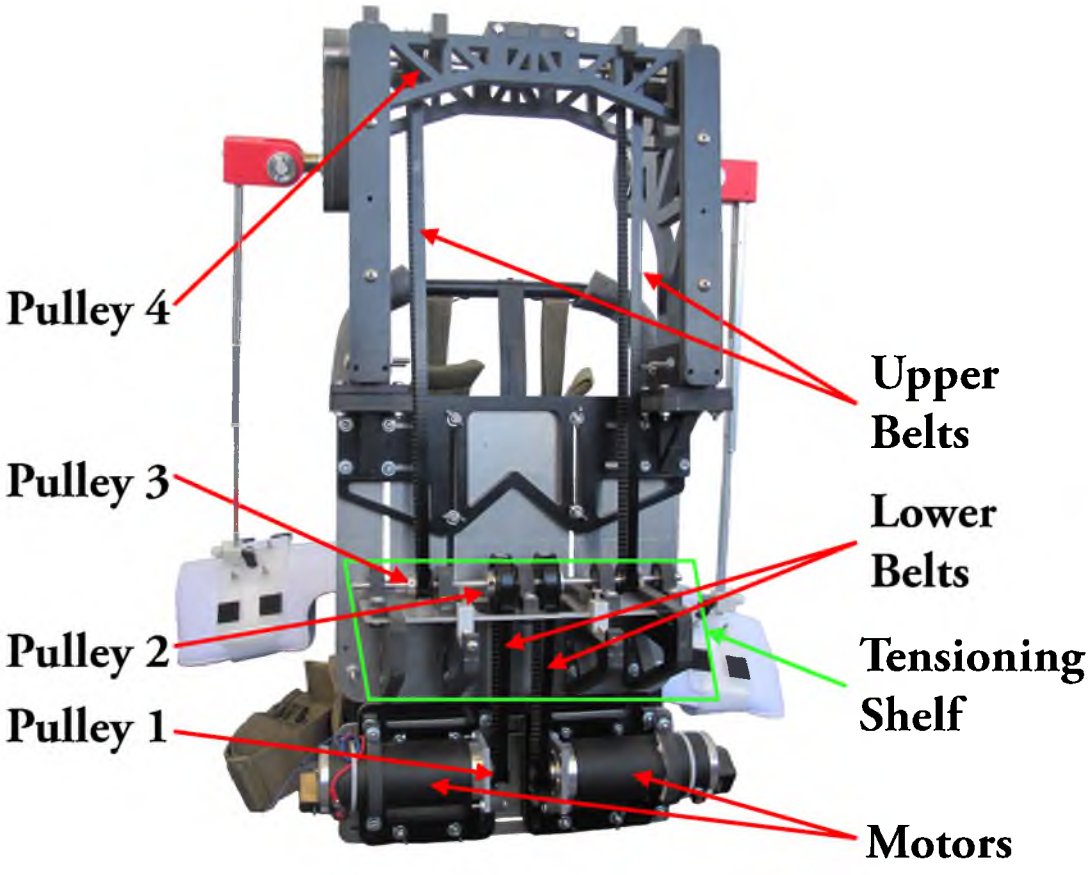

Figure 4.1. The timing-belt subassembly is located on the back of the ALICE frame. For each arm, there are two stages of belts, with two timing pulleys on each stage. The timing pulleys are numbered sequentially from the motors to the threaded capstan's shaft. The tensioning shelf is also highlighted.

and a gear ratio greater than 1 represents an amplification of the motor torque. The timing pulleys are numbered sequentially from closest to farthest from the motor.

The timing pulleys have surface contact between themselves and the shafts on which they are mounted. The surface contact allows the clamping force to be distributed over a large area of the shaft, as opposed to the use of set-screws that can wear grooves or loosen over time. The contact quality is good enough so that the timing pulleys resist slipping between themselves and the shaft, thus ensuring good torque transmission.

In conjunction with the timing pulleys, the timing belts transfer power from the motor shaft to the capstan drive. The timing-belt system uses belts that are sufficiently wide for withstanding belt-teeth deflections incurred by torque transmission. Preventing belt-teeth deflections is important in guaranteeing that the belts do not skip over the timing pulleys, thus keeping torque transmission effective.

The last member of the timing-belt system is the tensioning shelf. Its final design is seen in Figure 4.2. The tensioning shelf is located on the back of the UWEAR and lies between the lower and upper belts. The tensioning shelf carries bearings that hold shafts, which are used for transmitting torque. The tensioning shelf serves two purposes: it helps prevent slipping in torque transmission by tensioning the belts on the pulleys, and it facilitates easy assembly by allowing the belts to be put on the pulleys in a low-tension state.

The tensioning shelf is adjustable in two directions; the shelf's vertical and anteroposterior positions are both adjustable. The shelf has mounting screws that are inserted in slots in the aluminum back plate. This allows for it to be positioned at different heights on the user's back. The adjustability of the shelf's height makes the design flexible in choosing timing-belts. The mounting screws also let the tensioning shelf be positioned such that it is at the common point where the upper and lower belts meet. Then, the shelf can be anchored and can serve as a foundation for stretching the belts onto their pulleys. Adjusting the dorsal screws of the tensioning shelf draws it away from the user's back. This stretches the belts, which gives them more gripping force on the pulleys. The belts can be added to the pulleys loosely and then be tensioned to the right amount.

The tensioning shelf also aids in assemblability by providing adjustabililty in the mediolateral positions of the pulleys. This horizontal adjustability of the pulleys on their respective shafts makes it so the individual pulleys need only be in line within their own stage. That is, not all four pulleys need to be aligned, which removes the need of orienting the motor shaft to lie directly beneath the threaded capstan shaft. This design choice also

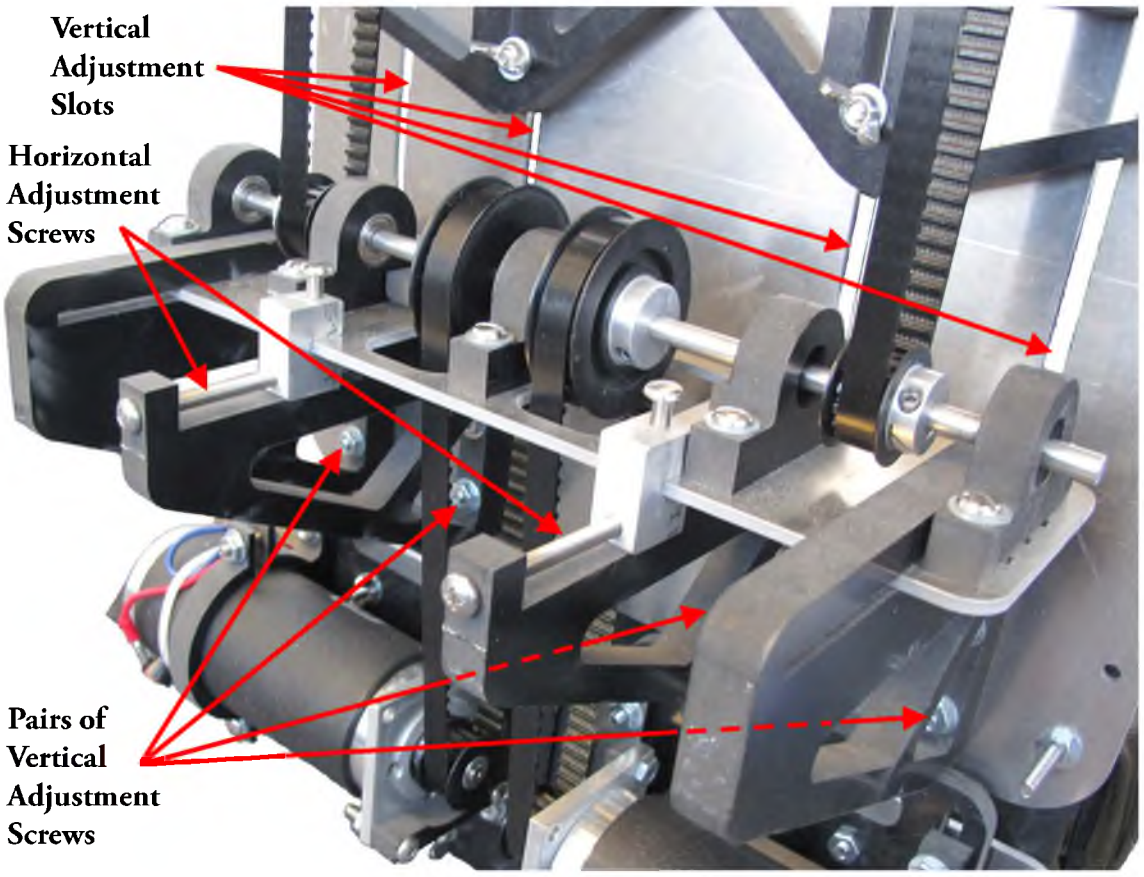

Figure 4.2. A close-up of the tensioning shelf. This device facilitates the assembly of the timing-belt system, and it keeps the belts taut, which ensures good torque transmission. The device has two DOF of adjustment (horizontal and vertical), so the lower and upper belts can be tensioned independently.

allows the motor shafts to be pointed inward, which removes the risk of the user's hand or arm making contact with the moving parts during normal arm swing.

4.1.3 Capstan Drive

The last member of the power transmission is the capstan drive. Its purpose is to take the output of the timing-belt system and add an additional stage of torque amplification for the arm-swing mechanism, in a backdrivable and backlash-free fashion. The inspiration for using the capstan drive comes from "haptic paddle" designs [24, 25]. The capstan drive is composed of a sector pulley, steel wire, a threaded capstan, and a tensioning block (as shown in Figure 4.3). The threaded capstan receives torque from the timing-belt system. It then transmits that torque to the sector pulley via the steel wire that is wrapped around both components. The shaft of the sector pulley then serves as the driving input to the

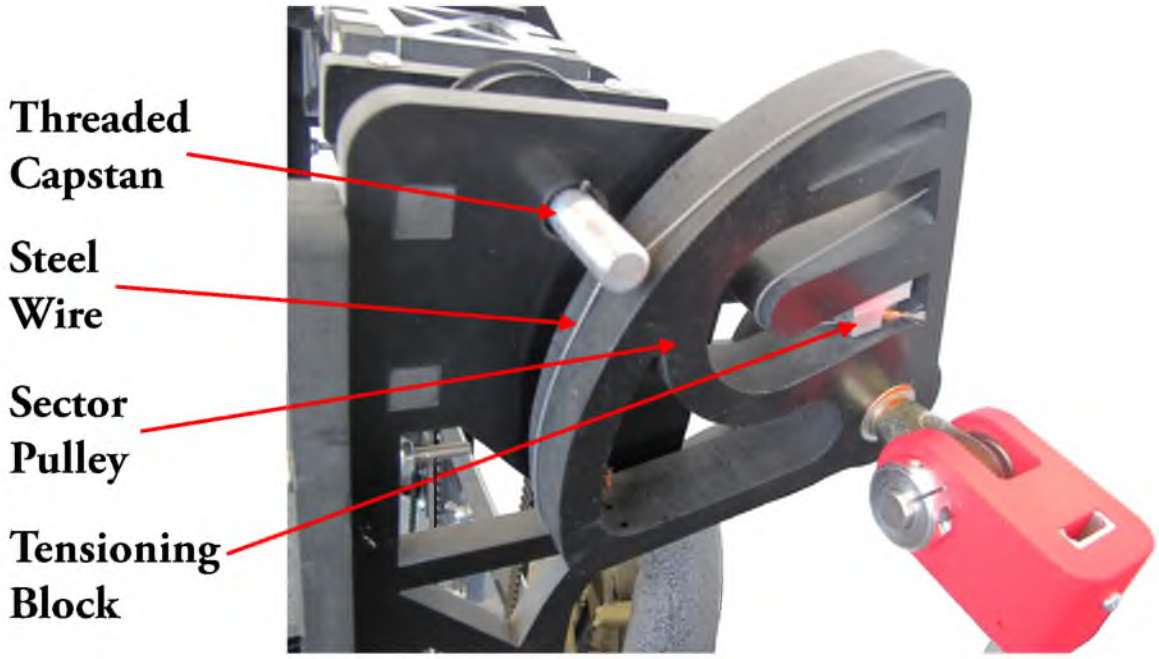

Figure 4.3. The capstan drive includes the threaded capstan, steel wire, sector pulley, and tensioning block.

arm-swing mechanism (described in Chapter 3). The tensioning block sits inside the sector pulley and helps maintain the tension in the wire.

The threaded capstan is the first portion of the capstan drive, and it is mounted on the output shaft of the timing-belt system. The threaded capstan receives torque from the timing-belt system and transmits it via steel wire. The steel wire is wound around the threaded capstan and connects to the accompanying sector pulley. The chosen thread of the threaded capstan should be such that it allows the steel wire to sit entirely within the threads of the threaded capstan, which helps keep the wire wrapped tightly. The number of times the wire is wrapped should be sufficient for providing enough friction to resist slipping between the threaded capstan and the wire. The axial length of the threaded capstan must be long enough to allow the steel wire to travel for the sector pulley's entire range of motion without unraveling.

The sector pulley is the second portion of the capstan drive. The sector pulley is moved by the steel wire, which anchors into the sector pulley's profile. The axis of rotation for the sector pulley forms the input to the shoulder joint of the underactuated arm-swing mechanism, O_m, defined in Chapter 3. The ratio of the sector-pulley and threaded-capstan radii determine the gear ratio for the capstan drive. The gear ratio, k_{CD} can be described by the following equation:

$$k_{CD} = r_{sp}/r_{cap} \tag{4.2}$$

where r_{sp} is the radius of the sector pulley and r_{cap} is the radius of the threaded capstan. With k_{CD} now defined, an expression for the gear ratio of the entire power train, k_{PT}, can be defined:

$$k_{PT} = k_{TB}k_{CD} \tag{4.3}$$

which uses the previously defined parameters.

The arc length of the sector pulley determines the angular range of motion of the underactuated arm-swing mechanism in the flexion/extension DOF. The sector-pulley arc length permits the user to flex/extend their shoulder in a range greater than what is expected for normal gait arm-swing trajectories. The larger range of motion allows the user to move uninhibited and comfortably while not performing rehabilitative exercises.

The steel wire anchors into the profile of the sector pulley through anchoring holes. These holes accomplish two purposes: they provide adequate reaction forces to keep the wire tensioned and they grant the wire a proper approach to the threads on the threaded capstan. The quality of the approach for the wire is dependent on the holes' positions along the thickness of the sector-pulley material. When the sector pulley is at its flexed/extended range-of-motion limits, so is the wire on the threaded capstan (as shown in Figure 4.4). The line that the wire follows from the threaded capstan to the closest anchoring hole should

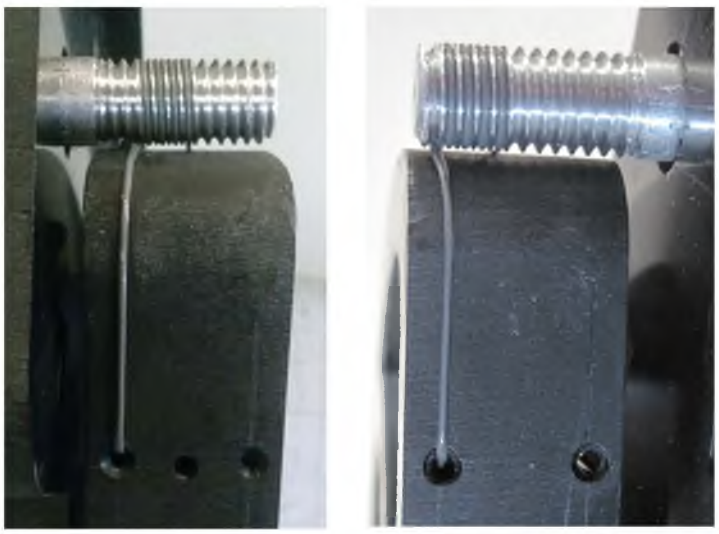

Figure 4.4. The alignment of the anchoring holes and the thread of the threaded capstan, for both the (a) flexed and (b) extended extremes of the sector pulley, ensures that the wire does not skip threads.

be perpendicular to the thread-capstan axis, allowing the wire to wrap straight onto the thread. This helps keep the wire from running over neighboring threads, which may occur if the wire enters at a skewed angle.

A tensioning block is used to tension (and retension) the wire of the capstan drive. The block lies inside of the sector pulley profile (shown in Figure 4.5) similar to a PHANToM haptic interface [26]. This block acts as an adjustable anchor point for one of the wire ends. Its adjustability arises from its tapped hole and the screw that threads into it. This adjustability is useful for removing slack that may be introduced into the wire after prolonged use of the UWEAR. The flat upper surface of the block prevents it from rotating relative to the sector pulley. The pilot hole is created such that the finished tapped hole has 75% thread engagement. A high thread engagement is important for preventing the threads from yielding and failing from the applied tensile force.

4.2 ALICE Frame and other Support Structures

The ALICE backpack frame comprises a metal frame and shoulder and waist straps, as seen in Figure 4.6. The ALICE frame has a lightweight (3.8 lbs) design since it is intended for infantry [27]. This helps keep the UWEAR nonenclosing and portable. The frame is adequately strong to bear the weight of the UWEAR's remaining components, which allows the entire mechanism to be wearable and portable.

The metal frame and fastening straps help keep the ALICE frame secure on the user's back. This helps ensure that the torques from the torque input induce arm motion and not movement of the UWEAR relative to the user's back. A chest strap spans the shoulder

Figure 4.5. The tensioning block sits inside the sector pulley profile.

Figure 4.6. The ALICE frame is important for providing a foundation for the UWEAR. Its rigidity and adjustable straps help the torque transmission remain efficient.

straps. The chest strap, as it is tightened, draws the shoulder straps away from the sides of the user's body. This helps remove the risk of rubbing that can occur between the user's arms and the shoulder straps.

The ALICE frame has a waist strap that is worn across the hips. The waist strap assists in bearing the weight of the whole UWEAR when there is no weight-support system present so that the entire weight is not felt solely on the upper body of the user. When the UWEAR is used in conjunction with a weight-support system, the straps of the ALICE frame can be adjusted to permit a rehabilitation harness to be worn underneath, as seen in Figure 4.7. Additionally, the waist strap helps keep the structure on the user's torso and away from their legs, keeping the legs free of interference from the device.

The majority of the UWEAR's structural pieces are placed behind the user on the ALICE frame. They are fastened on aluminum plates that are attached to the ALICE frame. The additional structures are constructed from ABS plastic, which is chosen for its strength and weight. They support the kinematically important components of the UWEAR and keep the UWEAR effectively rigid to limit unmodeled deflections.

There are two structural components that support the arm links of the UWEAR; they are referred to as the lateral supports. The lateral supports, as seen in Figure 4.8, house

Figure 4.7. The ALICE frame straps can be adjusted to allow a rehabilitation harness to be worn with the UWEAR with a weight-support system.

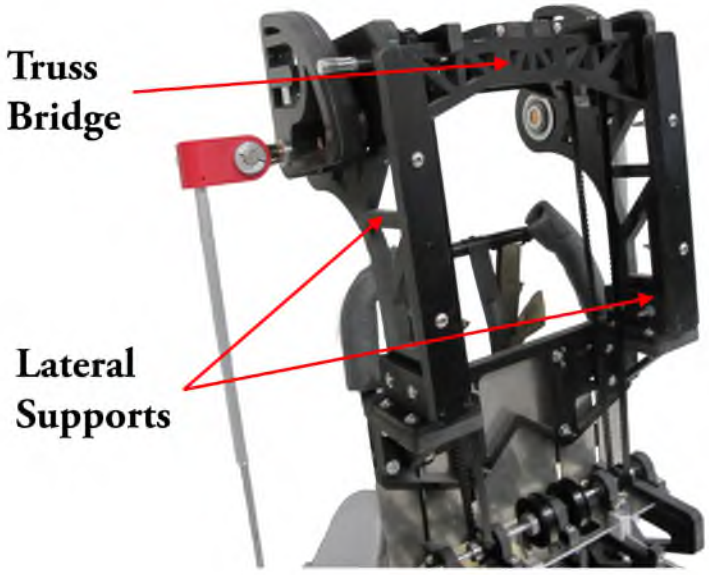

Figure 4.8. Additional supporting structures are important for the UWEAR's performance. They include the lateral supports and the truss bridge. The lateral supports act as a foundation for the arm assemblies. The truss bridge helps the whole upper structure remain rigid.

large bearings, which serve as the axes of rotation of the sector pulleys and the powered input axes for the arm-swing mechanisms. The supports allow the torques to be applied to the shoulder joints and arm links of the UWEAR. The lateral supports are placed apart with enough distance to permit the user's head to lie between them without any contact. The structures are positioned far enough back so they do not appear in the user's peripheral vision while the neck is relaxed. Keeping the structures out of the peripheral vision helps the user feel nonenclosed.

The truss bridge connecting the adjacent lateral supports is an important structural component. The bridge shown in Figure 4.8 stabilizes and reduces the deflection at the tops of the lateral supports when torques are applied. There are additional pieces of ABS plastic fastened to the posterior border of the lateral supports, which, along with the truss bridge, help make the support structures act as one rigid foundation. The rigidity of the structure as a whole helps maintain torque transmission efficiency, as well as sensor/arm collocation.

CHAPTER 5

DESIGN PARAMETER SELECTION

The previous chapters discuss the UWEAR's design concepts. This chapter uses the results of Chapters 2–4 to synthesize the design of a prototype device. First the independent parameters are selected, followed by the dependent parameters. Afterward, the final remaining design decisions for the power train are described.

5.1 Independent Parameters

As previously discussed in Chapter 2, the arm was modeled as a double pendulum and was simulated with typical arm-swing trajectories, resulting in an idea of the maximum torque magnitude required at the shoulder joint as well as where in the trajectory the maximum torque is needed (see Figure 2.2). It is noted that the absolute maximum torque occurs when the shoulder is fully flexed in its trajectory (i.e., $\theta_s = 10°$). The knowledge of where maximum torque occurs can be applied to select γ, which is the angular offset from vertical between the user's shoulder axis (O_s) and the mechanism's powered axis (O_m), shown previously in Figure 3.7. This knowledge can be used to choose γ so that when the user's shoulder angle is equal to gamma, the user's upper arm and the mechanism's prismatic arm link are parallel. When this is the case, the forces that are exchanged at the arm-cuff connection point, O_c, are purely perpendicular to the user's arm. That is, all the transmitted force is spent in rotating the user's upper arm about the shoulder, and no force is wasted to push/pull the arm cuff along the user's arm. This reaffirms the conceptual design decision to locate the powered axis of the underactuated arm-swing mechanism above and behind the user's head. The selection of γ provides a "solution line" of possible locations of O_m radiating outward from the user's shoulder axis; however, it does not provide its exact location. The location of the underactuated arm-swing mechanism's powered axis will be discussed later in this chapter.

Another parameter chosen independently of any other is the length of the user's upper arm segment from the shoulder to the arm-cuff connection, R. It could be estimated as

a proportion of the user's total height, but it can also be measured directly after the user dons the device. At the end of the length R lies O_c, the connection point of the mechanism to the user's arm, which is the location where forces are exchanged between the user and the mechanism. For the calculations in this chapter, R is assumed to be equal to 8.85 in (22.5 cm), which is a reasonable length for a subject 1.9-m tall with a mass of 100 kg, which we determined earlier to be our most demanding user (see Chapter 2).

Another independent parameter to be considered is the location of the user's center of mass. From previous research, the location of the human's center of mass is at 41.4% of the person's height measured down from the top of the head [21]. The center of mass is important in considering the total inertia of the combined Human-UWEAR system.

5.1.1 Motor Selection

Choosing the right motor is essential for obtaining the desired performance of the UWEAR. This section addresses the importance of the different motor requirements: the mass, dimensional size, backdrivability, and torque.

The first criterion that we considered for motor selection is the mass. Of all the components in the UWEAR, the two motors are expected to be most massive. The desired motor should be as light as it can be; however, favoring a lighter motor that does not provide enough torque is unacceptable. The primary concern is to minimize inertia, rather than weight, since it is anticipated that the UWEAR's weight will be compensated in practice (i.e., on a body-weight-support treadmill).

The next motor selection criterion is the dimensional size of the motor. Spatially, the motor should not extend far past the lateral borders of the ALICE backpack. Passing this boundary may obstruct and disrupt the user's arm swing and gait. Also, the motors cannot be so long that they pass the midline on the back of the mechanism. Minding the midline is important for allocating space between the motor shafts to prevent interference between the motors, so the motors can be placed symmetrically with respect to the midline at the same vertical position.

In order for the UWEAR to be unconstraining on the user's motions while unpowered, the selected motors need to be backdrivable. Backdrivability is the quality of being able to be moved relatively freely when applying a torque input to the motor's output shaft. It is our desire that the user be able to move their arms without feeling a large inertia or braking force preventing movement. Often, motors intended for the generation of large torque are sold with an attached planetary gear system, which amplifies the rotor inertia by many

times and adds significant friction. These gear systems are often nonbackdrivable and thus should be avoided.

Motor torque is the most important specification in recreating the arm trajectories that occur during normal walking. A poor motor selection with regards to torque can cause many problems. If the motor is too weak, these include not assisting the user enough or damaging the motor. If the motor is too strong, the user is put at greater risk of potential injury in the event of system failure. Research done by [9], [10], [22], and [23] suggest that the required shoulder torque is anywhere from 2.2 N·m to 12 N·m. For the restrictions placed on the UWEAR by mass, size, and backdrivability, it is unrealistic to expect that the selected motors can meet this requirement directly. The limited motor torque necessitates a mechanism to amplify the torque.

A number of motors were surveyed to see if they met the size, weight, and backdrivability requirements, then the motor that had the highest continuous stall torque was chosen. Of all the motors surveyed, the Brush Type DC Servo Motor from Servo Systems (#23SMDC-LCSS-500) follows all the specified design guidelines. It is a direct-drive motor, and its continuous stall torque is 0.388 N·m. One motor weighs 3.5 lbs (1.60 kg). The combined weight of the two motors account for 26.0% of the total weight of the UWEAR (26.9 lbs or 12.2 kg). The weight of the motors does not prevent the UWEAR from being lightweight and portable.

After the motor was selected, a brief calculation was done to examine if the UWEAR can be qualified as low-powered compared to the current exoskeleton-type technologies available for upper limb rehabilitation, which are typically strong enough to carry the user's limbs. We evaluated the UWEAR's ability to provide torque to hold the user's arm flexed at 90 degrees, where the torque from gravity is greatest. Using the mass parameters of our most demanding user, the shoulder torque required to hold the arm is 17.8 N·m. Next, the maximum effective shoulder torque that the UWEAR can produce in this same arm configuration was calculated. The geometry parameters for the UWEAR defined in the reminder of this chapter were used since they affect the nonlinear gear ratio between the sector-pulley and the effective shoulder torques. Using the maximum continuous stall torque of 0.388 N·m, the maximum effective shoulder torque the UWEAR can produce is 16.0 N·m, which is less than the shoulder torque required for suspending the arm flexed at 90 degrees. Thus, we refer to the UWEAR as a "low power" device, in that, while capable of generating arm swing, it is incapable of the type of support that is typical of more powerful upper limb exoskeletons.

5.1.2 Timing-Belt System Selection

As discussed in Chapter 4, a timing-belt system was chosen to assist the selected motor in providing sufficient torque to the user's shoulder while also granting the ability of providing torque at a different location than the motor's output shaft. Timing-belt systems are backdrivable, backlash free, and lightweight. The diameters and width were considered as timing-pulley and timing-belt options were investigated. With a goal of maximizing gear ratio, timing pulleys were chosen with pitch diameters, in inches, of $d_1 = 0.891$, $d_2 = 1.846$, $d_3 = 0.891$, and $d_4 = 1.846$. These pitch diameters result in a gear ratio of $k_{TB} = 4.30$. The belts were chosen to have a width of 0.375 in (9.525 mm), and the pulley width was chosen to accommodate belts of that size (0.438 in, 11.11 mm). The timing pulleys were selected from SDP/SI, and the timing belts were chosen from McMaster-Carr and have the following part numbers:

- 1.846-in pitch diameter timing pulley, #A 6H 3-29DF03708
- 0.891-in pitch diameter timing pulley, #A 6H 3-14DF03708
- 3/8-in upper timing belts, #1679K149
- 3/8-in lower timing belts, #1679K33

5.1.3 Steel Wire Selection and Threaded Capstan

The design of the threaded capstan and the selection of the steel wire were performed simultaneously, in an iterative manner, since each one significantly informs the other. The diameter of the steel wire affects the design of the threads on the capstan, and the diameter of the capstan affects the loading on the steel wire.

The diameter of the threaded capstan is bound by two design parameters. It is desirable to minimize the diameter to increase the gear ratio of the capstan drive. The lower boundary for the size of the threaded capstan comes from manufacturability concerns. The last stage of timing pulleys has a shaft on which the threaded capstan is mounted. The timing-pulley shaft diameter of 0.25 in (6.35 mm) has been chosen previously. It is necessary to have sufficient material between the threaded capstan's minimum diameter and the outer diameter of its mounting shaft. With these limitations in mind, a 0.5 in (12.7 mm) outer diameter is chosen for the threaded capstan. The radius of the threaded capstan, which is used in subsequent calculations, is $r_{cap} = 0.25$ in (6.35 mm).

The steel wire is used to transmit power between the threaded capstan and sector pulley. One important design feature of the wire is its flexibility; a wire that does not have a sufficiently small bending radius can fail to wrap tightly around the threaded capstan. A

7×19 strand core wire (#34235T27, McMaster-Carr) was chosen from a selection of steel wires recommended for controls and mechanical applications. The 7×19 core is more flexible and has better fatigue resistance than the other options. Choosing steel wire with adequate strength is also important to guarantee that the wire can bear the forces that it experiences during power transmission. The final selected steel wire has a breaking strength of 100 lbs (445 N). According to [28], it is recommended to preload the wire equal to the dynamic load encountered in the operation of the device; when this is the case, the maximum load encountered in the wire is equivalent to 1.5 times the dynamic load. The load on the wire is equal to the quotient of the output torque and the effective radius of the capstan. This relationship is solved for the corresponding motor torque that would cause the wire to break assuming the sector pulley is immovable, which is calculated as 0.438 N·m. This motor torque correlates to a motor current that is higher than can be supplied by the amplifiers controlling the motors; therefore, it is not possible with the current hardware that a destructive load can be applied to the wire.

We use the diameter of the steel wire to determine the thread of the screw on the capstan. The wire's ability to sit entirely within the threads helps keep the wire wrapped around the capstan. The whole drive fails if the wire unwinds from the capstan, so choosing the right thread is important. The final wire diameter of 0.037 in (0.940 mm) sits completely within a pitch of 13 threads per inch.

5.2 Dependent Parameters

The previous section discussed the independent design parameters that are driven by information from Chapters 2–4. This section discusses the other design parameters that rely on these previously mentioned independent variables.

5.2.1 Motor Placement

The motors are the heaviest component of the UWEAR. Therefore, it is important to consider their effect on the center of mass and rotational inertia for the entire system, such that the gait-rehabilitation purpose of the UWEAR is not compromised. Studies show that there are no differences in spatiotemporal gait parameters when loads are carried in low or high positions [29,30]. However, choosing the load (the motors in this case) to be placed at a lower position grants greater stability during walking than at a higher position [31,32]. Additionally, choosing a lower load position minimizes the rotational inertia of the whole system. From before, the location of the user's center of mass is at approximately 41.4% of their total height, measured from top of the head [21]; this is near the user's waist. We want

to place the motors near this height to minimize the displacement of the whole system's center of mass. However, there are other masses in the UWEAR that must be accounted for, including the more highly positioned additional supporting structures. The motors are placed lower, by the hips, to compensate for this additional mass since the hips are lower than the user's center of mass. The reduced displacement of the center of mass decreases the additional rotational inertia and in turn minimizes the dynamic moments that are felt at the user's lumbar spine [33].

The anteroposterior placement of the motor affects the moment felt at the lumbar spine. It is desired that this moment be minimized, so the motor is placed as close as possible to the ALICE frame. Any additional offset will increase the moment arm and thus the moment felt by the user. The horizontal distance from the motor shaft to the ALICE frame's dorsal surface was measured to be 2.1 in (53.3 mm) for the motor selected.

5.2.2 Developing the Power Train Geometry

This subsection discusses the determination of several coupled design parameters through the use of a governing equation for the device. It builds on the parameters discussed in the previous section of this chapter. The determination of the remaining power-train geometry allows for the remaining capstan-drive design parameters to be chosen.

The angle γ, which describes the angular offset from the vertical between the user's shoulder and the mechanism's sector-pulley axis, was chosen as $\gamma = 10°$ from information derived in Chapter 2. It was mentioned that the sector-pulley origin, O_m, would lie on this line indicated by γ, but it was not determined at that time at what distance it would be from the user's shoulder axis (O_s). In order for the sector-pulley origin to be located, the length D, from Chapter 3, needs to be determined (see Figure 3.7). The issue is that D is coupled with the sector-pulley radius, r_{sp}. A governing equation relating the power between power-train members is derived for the UWEAR when it is at the $\theta_s = \gamma = 10°$ configuration. In this configuration the force needed at the arm cuff to generate a desired effective shoulder torque τ_s with a factor of safety σ (i.e., $\tau_s\sigma/R$) must be equated to the force actually generated at the arm cuff by the UWEAR (i.e., $\tau_m/(R+D)$), and the motor torque τ_{mot} must be related to the torque generated by the arm-swing mechanism as in Chapter 3 (i.e., $\tau_m = \tau_{mot}k_{TB}r_{sp}/r_{cap}$). The result is an equation for the required sector-pulley radius:

$$r_{sp} = \frac{\tau_s\sigma(R+D)r_{cap}}{\tau_{mot}k_{TB}R} \tag{5.1}$$

Values for R, k_{TB}, and r_{cap} are defined previously. The safety factor σ applied to τ_s to ensure

good device performance in demanding torque scenarios. From Chapter 2, the maximum expected shoulder torque required to produced the desired arm-swing trajectory is 4 N·m. The parameter σ is chosen to be 3.0, making the product of τ_s and σ to be 12 N·m. This effectively puts the level of shoulder torque on par with the highest torque seen in the study done by [22] and three times as high as what the Chapter 2 inverse dynamics model predicts. The motor torque, τ_{mot}, is taken to be 0.30 N·m, which is the maximum continuous torque that can be supplied by the chosen motor.

Since (5.1) includes two unknowns, several design iterations were performed using a Rescue Randy mannequin (Simulaids, Saugerties, NY) as a model, until a suitable set of parameters was reached. The mannequin's height is 6 ft 1 in (1.85 m), which is similar in stature to our most demanding torque user. The final length of D, which locates the powered axis of the underactuated arm-swing mechanism (O_m), was chosen as 8.93 in (22.7 cm). The final radius of the sector pulley, r_{sp}, is 4.84 in (12.3 cm).

Now that D is chosen, geometric equations relating the underactuated arm-swing mechanism and the user's upper arm are derived to predict the length (L) and angle (θ_m) of the prismatic arm link. These equations reference the geometry shown in Figure 3.7. In this approach, it is assumed that the shoulder angle, θ_s, and not the sector-pulley angle, θ_m, is known.

To find L, the Law of Cosines is used on the triangle formed by O_m, O_s, and O_c. The resulting equation follows:

$$L = \sqrt{R^2 + D^2 + 2RD\cos(\gamma - \theta_s)} \tag{5.2}$$

Additionally, in order to predict L, the expected range of θ_s is required. One objective of the UWEAR design is to allow uninhibited motion even while not in operation, which will let the user move comfortably when they are not actively performing rehabilitative exercises. Therefore, we chose to provide the user with the freedom to flex their arms to 90 degrees from the resting position, as well as to permit the user to extend their arms as far back as possible, to 70 degrees. This is a total range of 160 degrees for the shoulder angle. This range of desired angles is used with (5.2) to find the minimum and maximum lengths of L. The values for R, D, and γ from before are used and yield lengths of 0.346 m to 0.452 m for L. A telescopic slide rail that adjusts to cover these ranges from MISUMI was chosen (#SAR230).

The derivation of the relationship that transforms θ_s to θ_m is described next. First, the angle ψ is found. It is part of an isosceles triangle formed by two sides of length R and the third by ρ. By summing all the interior angles of the triangle, ψ is as follows:

$$\psi = \frac{\pi - \theta_s}{2} \tag{5.3}$$

To find θ_m, the Law of Sines is used on the previously mentioned isosceles triangle to find the following relationship:

$$\frac{\rho}{\sin(\theta_s)} = \frac{R}{\sin(\psi)} \tag{5.4}$$

Next, the Law of Sines is used on the triangle whose sides are L_0, L, and ρ:

$$\frac{\rho}{\sin(\theta_m)} = \frac{L}{\sin(\alpha + \psi)} \tag{5.5}$$

The definition for α is the same used in Chapter 3. Equations (5.4) and (5.5) are each solved for ρ and then the resulting equation is solved for θ_m producing the following:

$$\theta_m = \arcsin\left(\frac{R\sin(\theta_s)\sin(\alpha + \psi)}{L\sin(\psi)}\right) \tag{5.6}$$

This relationship gives the angle θ_m for a given θ_s. This relationship can be used to map the desired range of shoulder angle into the necessary range of mechanism angle.

5.3 Determining the Remaining Capstan-Drive Parameters

The parameters D and r_{sp} are important in determining the remaining parameters and dimensions of the capstan drive. This last section uses the now-known values of D and r_{sp} to find values for the gear ratio of the capstan drive and power train, the sector pulley's angular range and arc length, and the threaded-capstan length and sector-pulley thickness.

Since the sector-pulley radius is now known, the gear ratio of the capstan drive and the power train as a whole can be quantified. The ratio of the sector-pulley radius to the threaded-capstan radius yields the capstan-drive gear ratio, k_{CD}. The capstan-drive gear ratio is found to be 19.4. The gear ratio of the entire power train, k_{PT}, is the product of the gear ratio of the capstan drive and the timing-belt system; it is found to be 83.2.

As discussed earlier, the distance between the user's shoulder axis and the sector-pulley axis, D, is an important parameter in the prismatic-arm-link to shoulder-angle relationship. Since the angle of the arm link also describes the angle of the sector pulley, the necessary angular range of the sector pulley can be determined. By using the previously discussed geometric relationships and desired range of shoulder-angle, the shoulder-angle range of 160 degrees is transformed and rounded up to 80 degrees for the sector pulley. This 80 degrees (1.40 rad) is then used to calculate the arc length of the sector-pulley:

$$s_{sp} = r_{sp}\Delta\theta_{sp} \tag{5.7}$$

This produces an arc length of 6.80 in (17.3 cm).

Knowledge of the arc length determines the length of the threaded capstan. The travel length of the steel wire is determined by comparing the sector-pulley arc length and the threaded-capstan circumference. With an arc length of 6.80 in and a threaded-capstan circumference of 1.57 in, the threaded capstan rotates 4.3 times on the sector pulley through the full range of motion. Every complete revolution of the capstan advances the wire axially by one thread. The calculated ratio of 4.3 is rounded up to 5 as a conservative measure of the number of threads traveled.

In addition to the threads traveled, a few more parameters need to be considered for the total travel length. The wire is wrapped four times around the threaded capstan to ensure there is enough friction between the capstan and the wire. The wire could be wrapped fewer times, but that would require the amount of tension on the wire to increase, causing more stretch. These occupied threads need to be included in the total threaded length of the capstan. Moreover, we add two additional threads on each end to act as a buffer so that unraveling never occurs. With these established concepts, the total thread length is calculated as

$$L_{total} = (T_t + T_o + T_s)/P \tag{5.8}$$

where T_t represents the number of threads traveled for the whole range of motion, T_o represents the number of threads occupied by the wire on the threaded capstan, T_s is the number of threads added as a safety measure to protect against unraveling, and P represents the pitch, or threads per inch, of the threaded capstan. Using the values discussed previously, the total number of threads required is 13, making L_{total} equal to 1 in (2.54 cm).

Now that the threaded capstan is completely designed, the last dimension of the sector pulley, the thickness, can be specified. The 1 in threaded length of the capstan translates directly into the sector pulley's required thickness of 1 in. When the UWEAR is at extrema in its range of motion, the wire wound on the threaded capstan is also at its extrema. These extreme points on the threaded capstan set the width for wire anchoring holes (described in Chapter 4) on the sector pulley.

CHAPTER 6

EXPERIMENTAL RESULTS

Two experiments were conducted in order to validate the functionality of the UWEAR before future use on its intended users (i.e., stroke and spinal-cord-injury patients). The first experiment examines the accuracy of the equations used to calculate human shoulder angles from measured sector-pulley angles. The goal of the second experiment is to assess if the UWEAR can provide adequate torque to its wearers for different trajectory types, arm-swing frequencies, and user-assistance levels. It also investigates whether or not a difference can be seen in user-assistance level through analyzing the motor-torque data and/or shoulder-angle data.

6.1 Donning the Device and Estimating Parameters Used in Shoulder-Angle Estimation

Both experiments in the following sections used a similar process for donning the UWEAR and measuring parameters that are used with the shoulder-angle equations derived in Chapter 3. With the help of another person, the user puts on the UWEAR on their back. The waist and shoulder straps are tightened to appropriate amounts. It is important to make the waist strap sufficiently tight so that the weight of the UWEAR is carried mostly by the user's hips and not their upper body. The chest strap is then fastened across the shoulder straps to pull the shoulder straps inward in order to provide clearance for the user's arms as they swing back and forth. Next, the arm cuffs are put on the user's upper arms near the biceps, such that they do not impede the flexion/extension of their elbow joints. The arm cuffs are secured on the user's upper arms by wrapping and fastening the hook-and-loop of the arm cuffs.

Once the UWEAR is donned, the parameters R, D, L_0, and γ are measured for each arm for use in the calculations derived in Chapter 3. A tape measure is used to obtain the lengths R, D, and L_0. The user is instructed to stand still with their arms relaxed at their

sides. R represents the distance between the user's shoulder-axis and the connection point of the arm cuff, which is measured at the threaded eyelet's axis of rotation. The length D is measured between the user's shoulder axis and the underactuated arm-link's powered axis. The initial length of the prismatic arm link, L_0, is measured by measuring the length of the telescopic slide bearings between the sector pulley's axis of rotation to the arm-cuff joint. The angle γ for both arms is estimated by measuring the vertical (b) and horizontal (a) distances to the sector pulley's axis of rotation from the user's shoulder joint. Then, the angle γ is found as $\tan^{-1}(a/b)$. The parameters for each arm are then loaded into the software, which uses the derived equations for predicting the user's shoulder angle. Table 6.1 contains the parameters used by each subject in the following experiments. However, only Subject 1 performed the sector-pulley to shoulder-angle relationship validation test.

6.2 Validation of Sector-Pulley to Shoulder-Angle Relationship

In Chapter 3, an equation relating the user's shoulder angle and the angle of the input joint of the underactuated arm-swing mechanism was derived. A simple experiment was used to verify the relationship by examining the errors between the calculated shoulder angle and the angle calculated by a motion-capture system. The UWEAR was placed on a healthy user wearing motion-capture markers. Optical encoders measured the motor shaft angle, which was then used with the analysis of Chapter 3 to estimate the shoulder angle. The shoulder angles were also calculated with motion-capture cameras. The arm angles were calculated by comparing the upper arm's orientation relative to the user's torso. The experiment consisted of two scenarios. In the first scenario, the user performed five static poses. In order to evaluate the errors under dynamic conditions, the second scenario comprised a trial in which the user swung their arms periodically.

For the static poses, the user started with his arms relaxed at his sides at the "zero" or vertical position. From there, the user performed four more poses and held the pose for 10 seconds while the motor encoder and motion-capture system recorded data. The four poses

Table 6.1. The parameters used for each subject in the tests contained in this chapter. The subscript L and R indicate the value for the left or right arm, respectively.

Subject	R_L (m)	R_R (m)	D_L (m)	D_R (m)	L_{0_L} (m)	L_{0_R} (m)	γ_L (°)	γ_R (°)
1	0.18	0.19	0.18	0.215	0.34	0.35	7	6
2	0.19	0.18	0.21	0.22	0.37	0.36	11	11
3	0.19	0.19	0.20	0.20	0.37	0.36	9	12
4	0.19	0.19	0.19	0.20	0.35	0.36	10	11

included fully extending both the arms, a semiextended pose, a semiflexed pose, and a fully flexed pose. The fully flexed and fully extended poses were limited by a combination of the user's anatomical range-of-motion and the UWEAR's range-of-motion. The semiflexed and semiextended poses were arbitrarily chosen by the user. The average angles selected by the subject for the fully extended, semiextended, zero, semiflexed, and fully flexed poses were, respectively, -32.0±4.1, -12.8±2.9, 0±0.3, 44.1±2.1, and 89.3±6.7 (mean ± standard deviation, in degrees). These posing trials were performed four times. Figure 6.1 shows a plot characteristic of the static poses scenario.

The arm angle data for the static poses was then prepared for analysis by removing the bias in the motion capture data's zero position so that both the angle calculated from the encoders and the motion capture started at the same position (i.e., 0 degrees). Next, the recorded poses were examined case by case for each trial. Equal time segments were chosen from the encoder and motion capture data for each pose. The data of interest were chosen from the time after the transient in shoulder angle, caused by changing poses, had decayed. Once the pose segments had been extracted, the encoder data were resampled to match

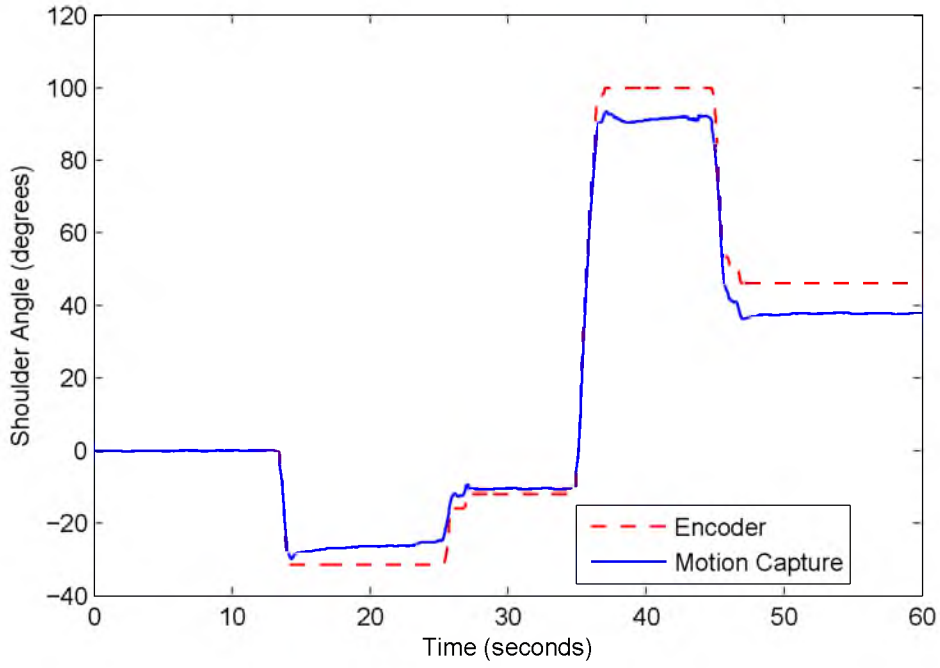

Figure 6.1. A recording typical of the sector-pulley to shoulder-angle relationship test for the static poses scenario. The shoulder angles calculated from the encoder readings are indicated by the dashed red line, and the shoulder angles from the motion capture data are indicated by the solid blue line.

the length of data points found in the motion-capture data. Then errors between the two signals for each pose segment were calculated as well as other statistics.

The absolute and relative errors (relative to the motion-capture data from each trial) were calculated for each pose in the static scenario. Figures 6.2 and 6.3 and Table 6.2 contain the results of the first scenario. The average errors are connected by dashed lines in Figures 6.2 and 6.3 with the vertical bars representing the standard deviations of the data. It can be readily seen that the relationship for converting sector-pulley to shoulder angles has nonnegligible error, with the average relative error never exceeding 17% in any case. Recall that the normal operating range of the UWEAR is from -30 degrees (extension) to

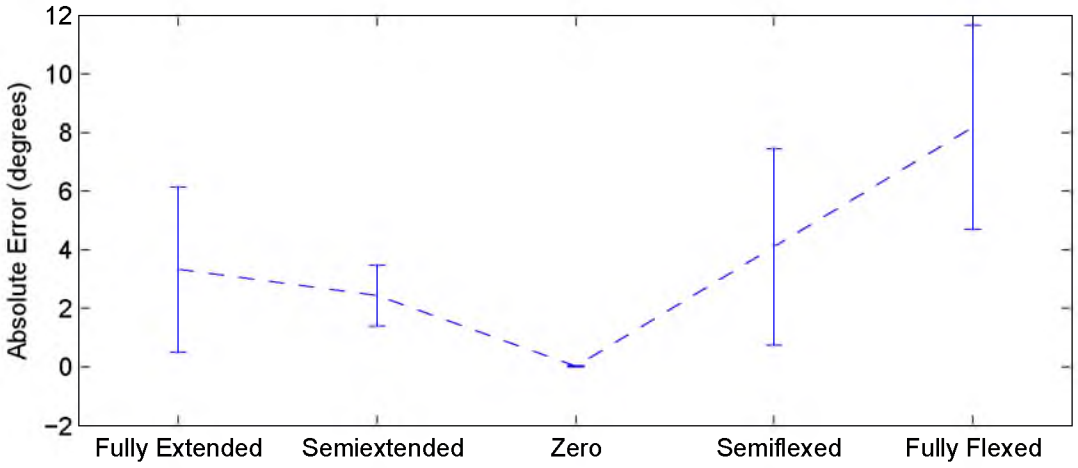

Figure 6.2. Average absolute errors and their standard deviations for each pose.

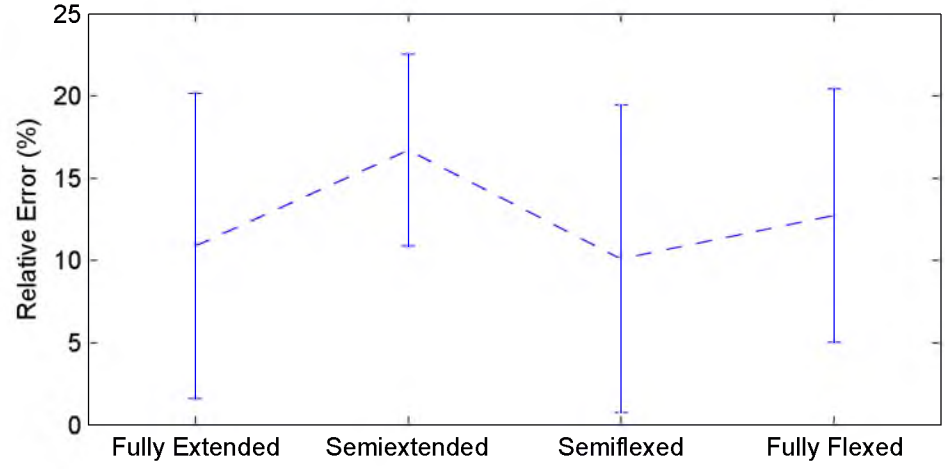

Figure 6.3. Average relative errors and their standard deviations for each pose. The relative errors are the absolute errors relative to the motion-capture data.

Table 6.2. Results of the experiment used to validate the sector-pulley and shoulder-angle relationship. The mean errors and their standard deviations are reported. The errors are calculated from the difference in angular measurement from the encoder and motion-capture data. The relative errors are relative to the motion-capture data.

Pose	Absolute Error (degrees)	Relative Error (%)
Fully Extended	3.3±2.8	10.9±9.3
Semi-Extended	2.4±1.0	16.7±5.8
Zero	0.02±0.02	N/A
Semi-Flexed	4.1±3.3	10.1±9.4
Fully Flexed	8.2±3.5	12.7±7.7

10 degrees (flexion), meaning that the larger flexion errors describe errors outside of the normal shoulder-angle range.

For the dynamic arm-swing scenario, the user started relaxed with his arms at his sides at the vertical position. After standing still for 15 seconds, the user moved his arms through his full range of motion, limited by his own anatomy and the UWEAR's range of motion, in a periodic manner until a minute had elapsed. This dynamic arm-swing trial was performed once. A characteristic plot can be seen in Figure 6.4. Only the absolute error between the motion-capture and encoder trajectories were calculated for the dynamic arm-swing scenario. The resulting absolute-error trajectory can be seen in Figure 6.5. The maximum shoulder-angle errors occur at the extrema of the arm motions when the arm is either flexed or extended well beyond what is typical of normal arm swing and are at most 12 degrees.

Evidence of the inaccuracy in the shoulder measurement using only the motor's encoder can be seen in Figure 6.1 starting at time = 14 s; the upper arm moves as the subject holds their pose according to the motion-capture system, but the encoders do not report any motion. Inaccuracy is the drawback of using only one sensor for estimating the shoulder angle. One source of inaccuracy is the human error involved when measuring the parameters D, R, L_0, and γ necessary for carrying out the geometric calculations. Additionally, there is a little slop in the bearings located at the underactuated arm-link mechanism's powered axis (i.e., the "flexion/extension" joint in Figure 3.2). By using a protractor, the bearing's angular slop in the arm links was measured to be 1.5 degrees. At time = 25 s, the upper arm has drifted so that there is a total error of 6 degrees in shoulder angle. It is likely that the major contributor of error is due to the approximate nature of the equations used for estimating the shoulder angle because those equations assume the shoulder joint to be a pin joint. In Figure 6.6, the amount of shoulder displacement for the corresponding

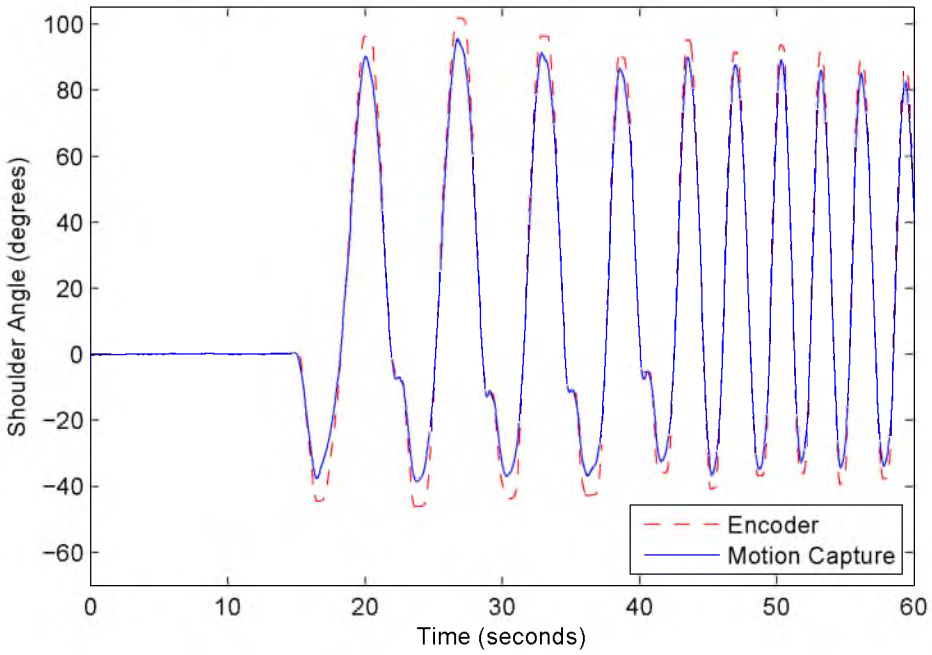

Figure 6.4. A recording typical of the sector-pulley to shoulder-angle relationship test for the dynamic arm-swing scenario. The shoulder angles calculated from the encoder readings are indicated by the dashed red line, and the shoulder angles from the motion capture data are indicated by the solid blue line.

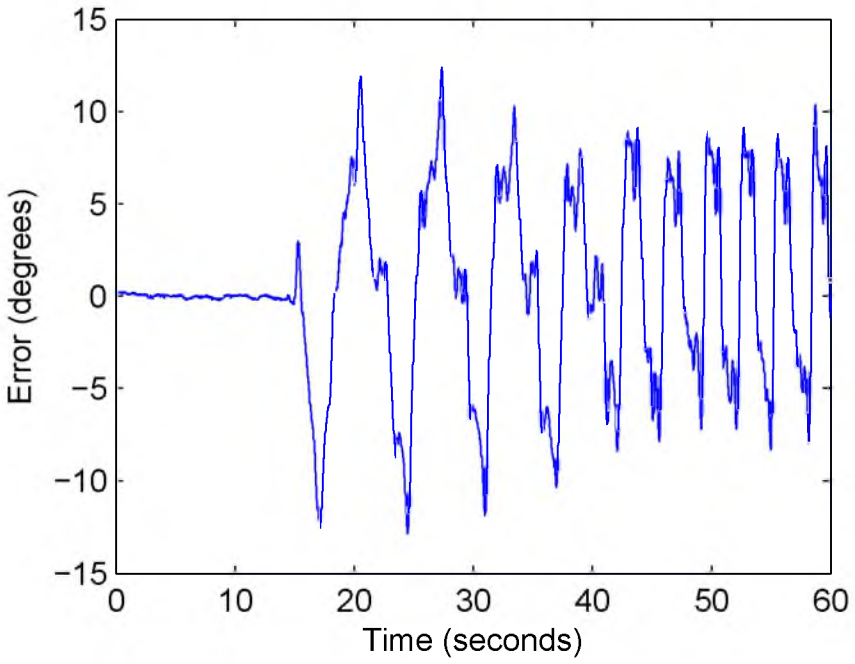

Figure 6.5. Absolute errors between the motion-capture and encoder data for the shoulder-angle prediction equations of the dynamic arm-swing scenario.

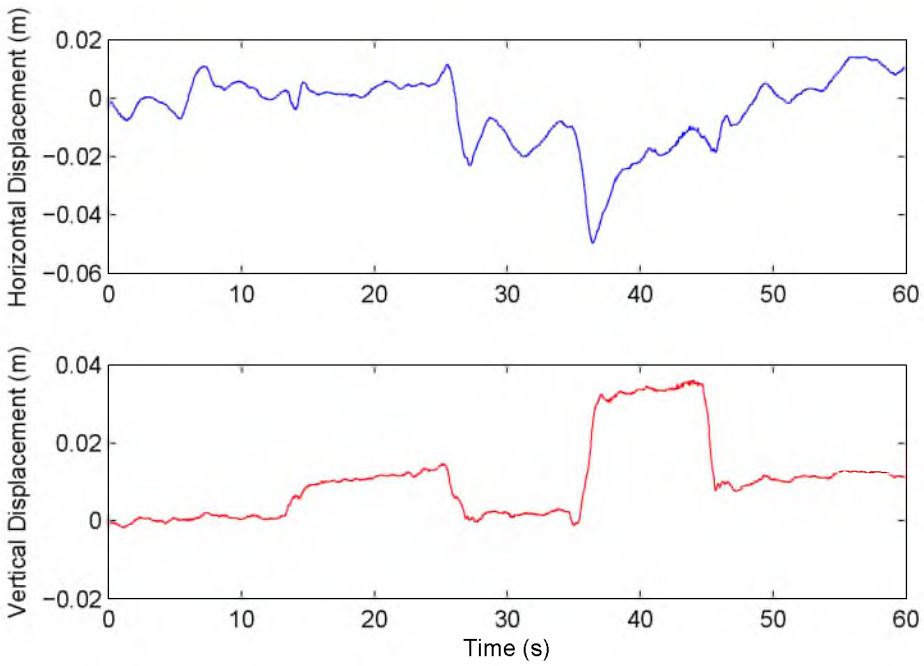

Figure 6.6. Plot of the horizontal (front to back) and vertical shoulder displacement as recorded by the motion-capture system corresponding to the data shown in Figure 6.1.

static pose trial is shown, with the largest displacements in either direction being nearly 4 cm. The shoulder displacement for the dynamic arm-swing scenario is seen in Figure 6.7, with a maximum displacement of approximately 6 cm in the vertical direction. The vertical displacement in particular seems to have a large influence on the error of the estimation equations since the large displacements correlate with the largest shoulder-angle errors for both the static and dynamic scenarios. As the user stretches out their arm while displacing their shoulder vertically, the user is able to change the angular position of their upper arm without the encoders sensing the change. Thus, if the UWEAR is to be used for arm-swing rehabilitation it should be understood that there could always be angular position errors of 5–10 degrees due to shoulder displacements. An interesting topic for future work would be to characterize the motion of the shoulder throughout the gait cycle, which would enable the arm-swing geometric model to be updated accordingly, which would almost certainly lead to improved predicting power.

A sensitivity analysis was performed in order to investigate the effect that inaccuracies in D, R, L_0, γ, and θ_m have on the accuracy in predicting the shoulder angle, θ_s, as it is calculated by (3.8). A local method was used for determining the sensitivities and potential errors in θ_s. The values for D, R, and γ are the ones previously defined for the most

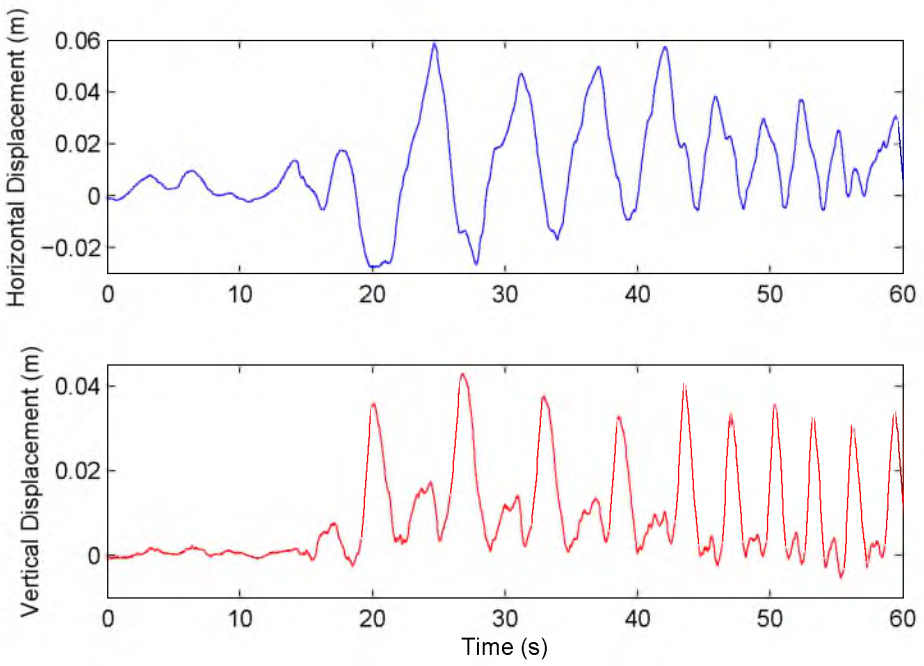

Figure 6.7. Plot of the horizontal (front to back) and vertical shoulder displacement as recorded by the motion-capture system corresponding to the data from the dynamic arm-swing scenario shown in Figure 6.4.

demanding torque user when it is at its resting position ($\theta_m = 0°$). The value for L_0 is found from (3.4); its length is 0.450 m.

The accuracy in θ_s can be described by the following matrix equation:

$$\Delta\theta_s = \left[\begin{array}{ccccc} \frac{\partial\theta_s}{\partial D} & \frac{\partial\theta_s}{\partial R} & \frac{\partial\theta_s}{\partial L_0} & \frac{\partial\theta_s}{\partial\gamma} & \frac{\partial\theta_s}{\partial\theta_m} \end{array} \right] \left[\begin{array}{ccccc} \Delta D & \Delta R & \Delta L_0 & \Delta\gamma & \Delta\theta_m \end{array} \right]^T \tag{6.1}$$

The partial derivatives with respect to the different independent variables represent the sensitivities to those variables at a fixed point, described by the previously defined values of the parameters D, R, L_0, γ, and θ_m. The elements in the transposed vector represent the accuracies of those variables when they are measured on the user as he wears the UWEAR. Table 6.3 contains the expected accuracies and calculated sensitivities and error

Table 6.3. This table contains the accuracies, sensitivities, and error contributions of the independent variables used in estimating the shoulder angle.

Variable	D	R	L_0	γ	θ_m
Accuracy	0.02 m	0.02 m	0.01 m	4.0°	2.0°
Sensitivity	-2.21 $\frac{\text{rad}}{\text{m}}$	-2.21 $\frac{\text{rad}}{\text{m}}$	2.22 $\frac{\text{rad}}{\text{m}}$	0.044	-0.088
Error Contribution (°)	2.54	2.54	1.27	0.26	0.18
Error Contribution(%)	37.4	37.4	18.7	3.83	2.65

contributions of the variables. The error in measuring both D and R accurately is taken to be 2 cm since finding the precise location of the user's shoulder center is difficult. L_0 is measured more accurately since the initial length of the arm link is measured entirely on the UWEAR, and the endpoints of L_0 are more clearly defined than those of the parameters that involve the user's shoulder joint. The angle γ is estimated from measuring the vertical and horizontal distances that are the legs to the triangle whose hypotenuse is D. The measurements of the vertical and horizontal offsets are done with a tape measure, and these measurements are done with an accuracy of 2.0 cm. In a worse case scenario of measuring γ, the maximum error is expected to be 6 degrees. The accuracy of the parameter θ_m is subject to the bearing slop, which amounts to 2 degrees rounded up. It is seen that the length measurements of D, R, and L_0 have the most influence in the shoulder-angle accuracy. The worst case accuracy in θ_s is calculated by summing the absolute value of each respective variable's product of the sensitivity and accuracy; it totals 6.8 degrees. The root-sum-square accuracy in θ_s is calculated to be 3.8 degrees. These errors in the shoulder angle are not as large as what was observed in the sector-pulley to shoulder-angle validation experiment. However, as discussed previously, those experiments involve additional error in the prediction of the shoulder angle due to the changing position of the shoulder joint.

6.3 Validation of Arm-Swing Generation

6.3.1 Design of the Experiment

An experiment was designed to examine the UWEAR's ability to generate arm swing in its users. The experiment examined different factors' effects on arm-swing generation, namely, arm-swing frequency, trajectory type, and user-assistance level. The main purpose is to see if the user-assistance level (i.e., if the user is passive or if the user attempts to swing their arms in sync with the mechanism) has any effect on the motor torque and shoulder angle for a range of different trajectories and frequencies. The experiment involved having the subjects stand, not walk, while wearing the UWEAR. The UWEAR's controller was used to swing the subject's arms on a sinusoidal shoulder-angle trajectory, starting from rest, while the shoulder angles and motor torque were recorded. The shoulder-angle data were examined by calculating the amplitude of the signal during each cycle. That is, for each period, the distance between neighboring shoulder-angle extrema was found and then divided by two. A total of 15 amplitudes were measued in each trial. The torque data was analyzed in two ways: by inspecting the torque signal's extrema in each period of arm swing and by examining the root mean square (RMS) value of the torque signal. When

the torque extrema was examined, only the minima were considered because the inverse dynamics model in Chapter 2 predicts the magnitude of the minima to be larger than the maxima. A total of 15 minima were taken in each trial. Figure 6.8 displays characteristic trial data recorded for motor torque and shoulder angle. The recorded torque and shoulder angle data were only considered after 5 seconds in order to remove any influence of the start-up transient.

Each trial has one of two arm-swing frequency scenarios for the sinusoidal trajectories. The arm-swing frequency was either 1.0 or 1.2 Hz. These two cases use frequencies that are typical of healthy walking cadences [34]. However, 1.2 Hz is a higher-than-normal frequency that represents the upper limit on walking frequency that the UWEAR should realistically encounter during rehabilitation tasks.

The trajectory type is another factor that changes each testing period. For each trial, the amplitude scales up from zero to a constant amplitude. Increasing the amplitude allows the UWEAR to smoothly and safely commence without any jarring torques on the user. The first trajectory's amplitude is typical of arm swing during walking [19]. In the first trajectory, the signal is offset at -10 degrees with an amplitude of 20 degrees. Moreover, this offset trajectory is what the UWEAR is optimized for since it has a maximum flexion and extension of 10 and 30 degrees, respectively. In the second case, the trajectory is symmetric about 0 degrees with an amplitude of 30 degrees. This trajectory is used to evaluate the UWEAR's performance in following trajectories for which it was not optimized.

The third factor varied in the experiment is user assistance. The two scenarios tested

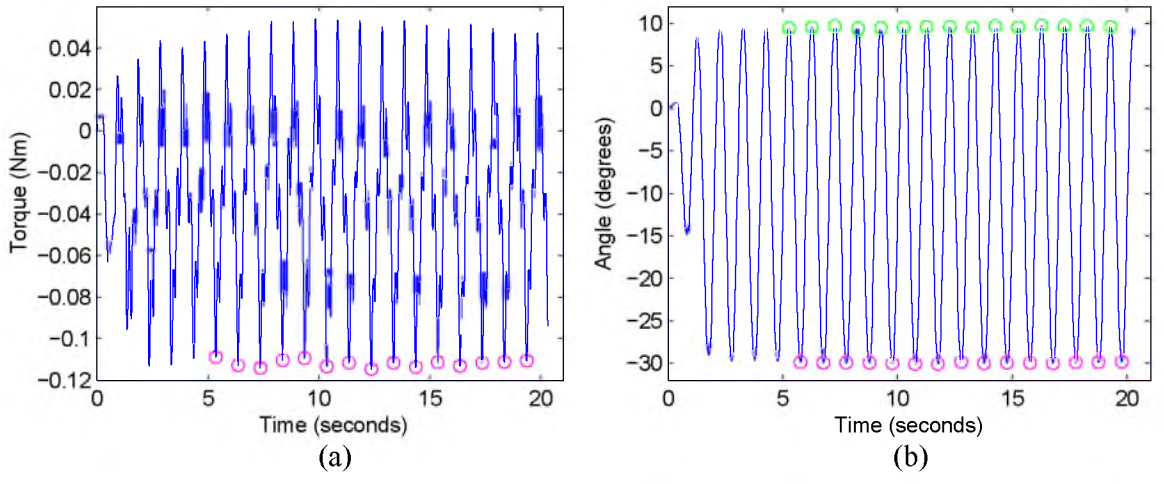

Figure 6.8. Characteristic plots of the arm-swing generation experiment for both the recorded (a) motor torque and (b) shoulder angle. The peak values used for analysis are circled.

are passive and assistive. In the passive scenario, the user lets the UWEAR move their arms without any voluntary muscle activity either helping or resisting motion. In the assistive scenario, the user moves their arms in an attempt to follow the UWEAR in its trajectory, based only on the haptic cues being perceived. Each combination of frequency and trajectory discussed above is tested under both the passive and assistive scenarios.

Four healthy male subjects were used to validate the function of the UWEAR; their heights and weights are listed in Table 6.4. A small set of subjects was used because we simply want to validate the functionality of the UWEAR; our goal is not to perform a human-subjects experiment to determine some quantity with statistical significance. Each subject performs a total of 16 trials, run for 20 seconds each. The trials comprise every combination of levels for each factor and they are performed in a random order. The tests are done in two periods. The first period tests the UWEAR with different frequencies and user-assistance levels for the offset arm trajectory for which the UWEAR was designed. The second period tests are equivalent except that the symmetric-about-vertical trajectory is tested. Each trial was performed twice.

Other hardware and software are necessary to complete experiments that validate the design of the UWEAR. They provide control and data recording capabilities for the experiment. A power supply purchased from Advanced Motion Controls (#PS2X3W24) is used to power the UWEAR through means of the Advanced Motion Controls Brush-Type PWM Servo Amplifier (#30A8C). The amplifier controls the motors by sending current to the motors indicated by a control voltage from the computer's data acquisition card (DAQ), which has a constant of $k_v = 0.3\,\mathrm{A/V}$. The commanded current is logged and multiplied by the motor's torque constant ($k_\tau = 0.09674\,\mathrm{N{\cdot}m/A}$) to give the amount of motor torque used to create arm-swing motions. The DAQ used is the Model 626 Multifunction Analog/Digital I/O by Sensoray. Additionally, the DAQ also receives information from the UWEAR's motor encoders. The encoder data are then transformed with the relationships derived in Chapter 3 to estimate the user's shoulder angles. The DAQ interfaces with the computer to

Table 6.4. Heights and weights of the individual test participants.

Subject	Height (m)	Weight (kg)
1	1.71	80
2	1.71	70
3	1.77	65
4	1.77	90

report these data to the accompanying software that controls the UWEAR. The computer software is created in C++. The program contains a control loop with data recording functions. The controller used is a combined feed-forward and PD controller, with PD gains of $k_p = 2.0\,\mathrm{N{\cdot}m/rad}$ and $k_d = 0.3\,\mathrm{N{\cdot}m/rad}$ for both arms. The feed-forward portion of the controller uses the dynamic simulation that is detailed in Chapter 2. It calculates the required shoulder torque from the desired trajectory and applies it in an open-loop fashion.

6.3.2 Results and Discussion

The results of the arm-swing generation experiment are contained in this subsection. Since many of the data in this chapter are represented with box plots, a brief introduction on how to interpret them is included here. Box plots show the distribution of the data. The red line in the center indicates the median of the data. The upper and lower blue edges that bound the box indicate the 75th and 25th percentile of the data, respectively. The dashed black lines above and below the boxes—the whiskers—extend to the most extreme data points that are not considered outliers. Outliers are plotted as red crosses, if they are present. The notches centered around the medians of the box plots indicate—with 95% confidence—whether or not the true median differs from another box depending on if the boxes' notches overlap.

Figures 6.9 and 6.10 show box plots of the calculated motor torque minima (i.e., the maximum absolute value) from the trials. The highest torque, for all the data, is never higher than $0.161\,\mathrm{N{\cdot}m}$. This is approximately half of the motor torque that can be provided by the selected motors. This suggests that for the current UWEAR prototype, the motors could be replaced with smaller motors that provide less torque but also weigh less, thus making the UWEAR prototype less burdensome to wear without a weight-support system. When comparing similar assistance levels and arm-swing frequencies, the absolute maximum motor torques for the symmetric trajectory are significantly larger than those for the offset trajectory, except for the assistive case at $1.0\,\mathrm{Hz}$. That is to be expected since the symmetric trajectory takes the arm through a larger range of motion by making the arm flex more at the shoulder. When comparing the box plots for the same trajectory, there is no significant difference in motor torque. It is interesting to see that there appears to be no significant difference between the assistive and passive levels of user assistance.

In order to investigate the lack of difference between the assistive and passive levels of user assistance, the controller efforts are examined. Plots containing the calculated PD, feed-forward, and total control efforts for the offset and symmetric trajectories for the 1.71-m-tall, 80-kg subject, for both user-assistance levels with an arm-swing frequency of

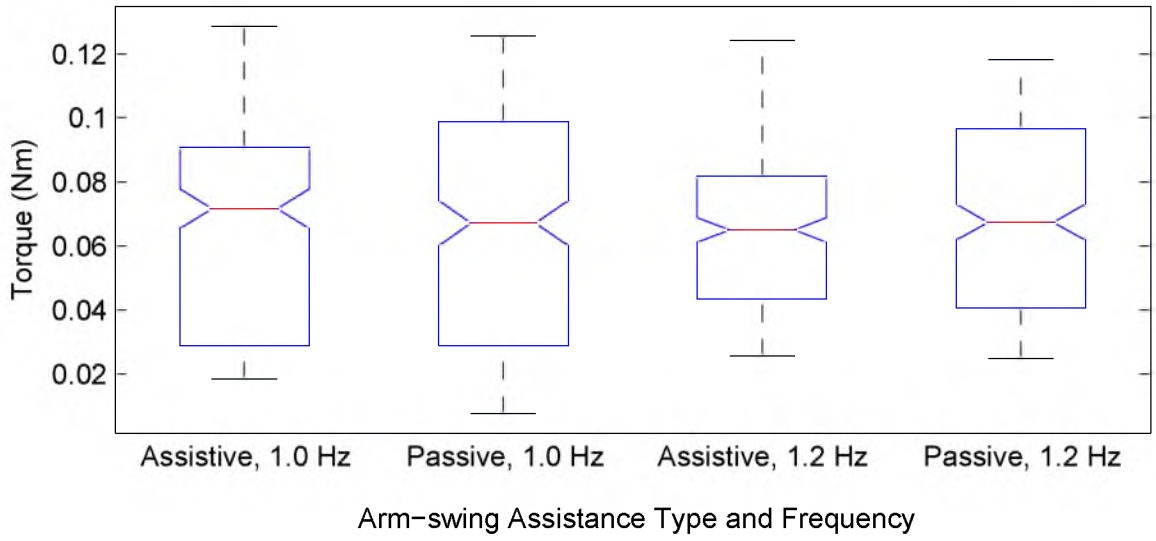

Figure 6.9. These box plots show the distribution of the calculated motor torque absolute maximums classified by assistance type and frequency for the offset arm trajectory.

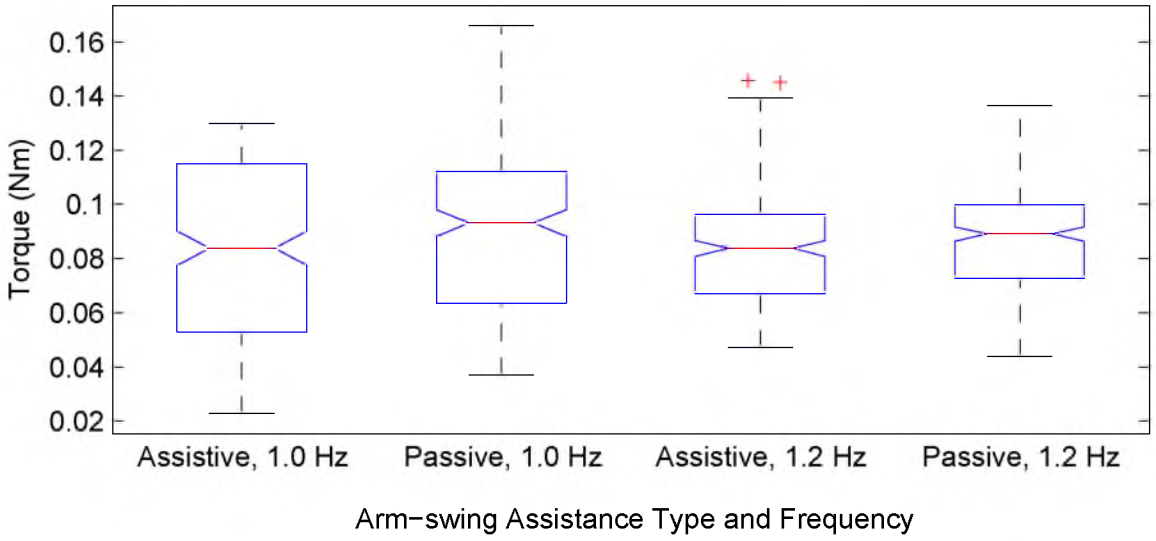

Figure 6.10. These box plots show the distribution of the calculated motor torque absolute maximums classified by assistance type and frequency for the symmetric arm trajectory.

1.0 Hz, are shown in Figures 6.11–6.15. The figures display the control efforts in terms of motor torque, except for Figure 6.11, which displays the efforts in terms of effective shoulder torque. This effective shoulder torque is the torque that would be applied by the user's shoulder to generate the motion if it were not for the UWEAR. It does not include any torque produced by the user themselves through muscles. Figure 6.11 is shown in terms of effective shoulder torque in order to make an easier comparison to the torque

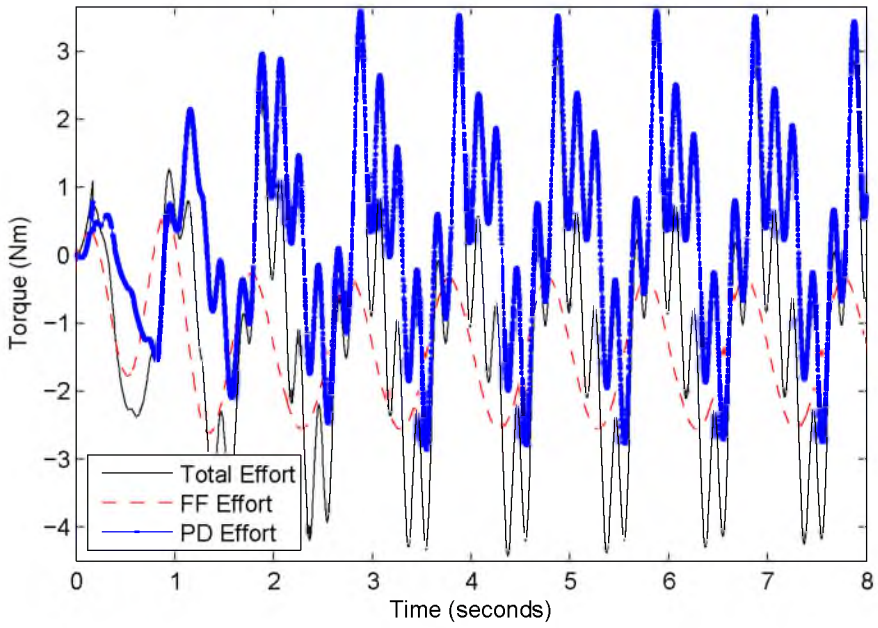

Figure 6.11. Plot of the feed-forward, PD, and total controller efforts (in shoulder-torque space) for the offset trajectory with an arm-swing frequency of 1.0 Hz and the user (1.71-m tall and 80 kg) acting passively.

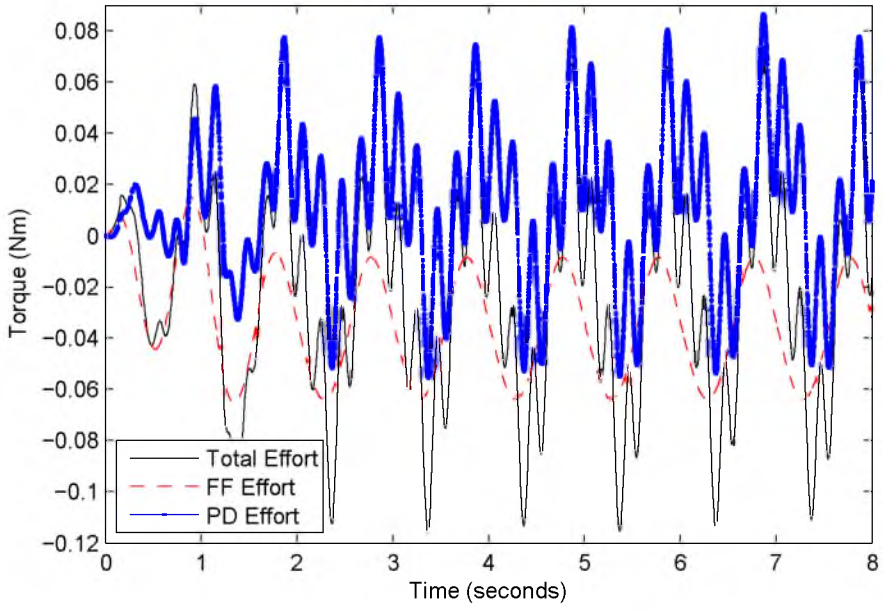

Figure 6.12. Plot of the feed-forward, PD, and total controller efforts (in motor-torque space) for the offset trajectory with an arm-swing frequency of 1.0 Hz and the user (1.71-m tall and 80 kg) assisting the device.

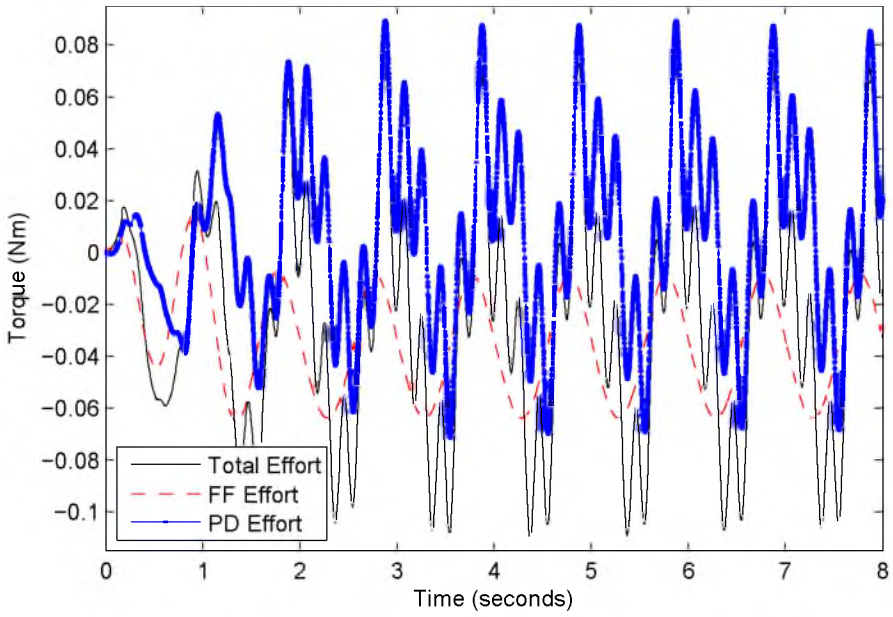

Figure 6.13. Plot of the feed-forward, PD, and total controller efforts (in motor-torque space) for the offset trajectory with an arm-swing frequency of 1.0 Hz and the user (1.71-m tall and 80 kg) acting passively.

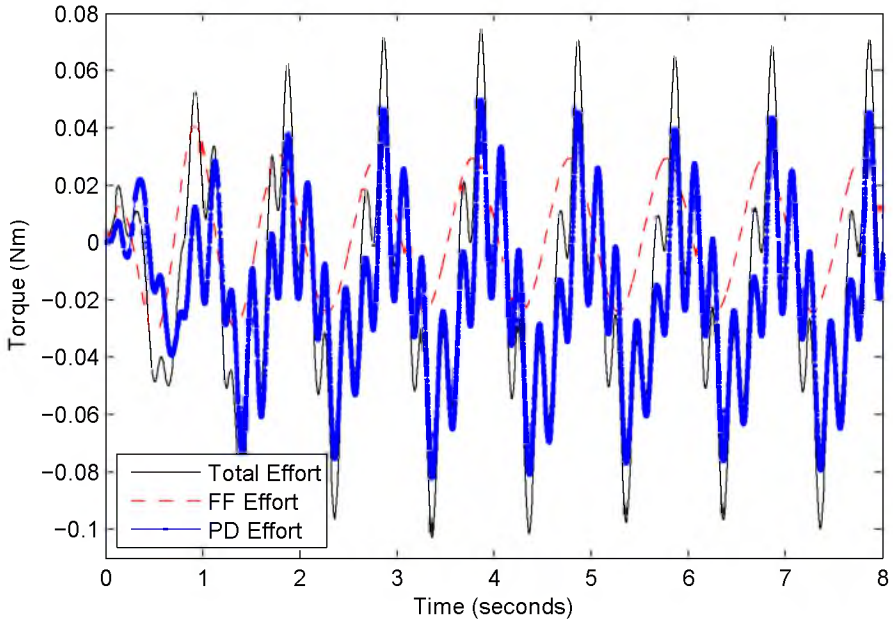

Figure 6.14. Plot of the feed-forward, PD, and total controller efforts (in motor-torque space) for the symmetric trajectory with an arm-swing frequency of 1.0 Hz and the user (1.71-m tall and 80 kg) assisting the device.

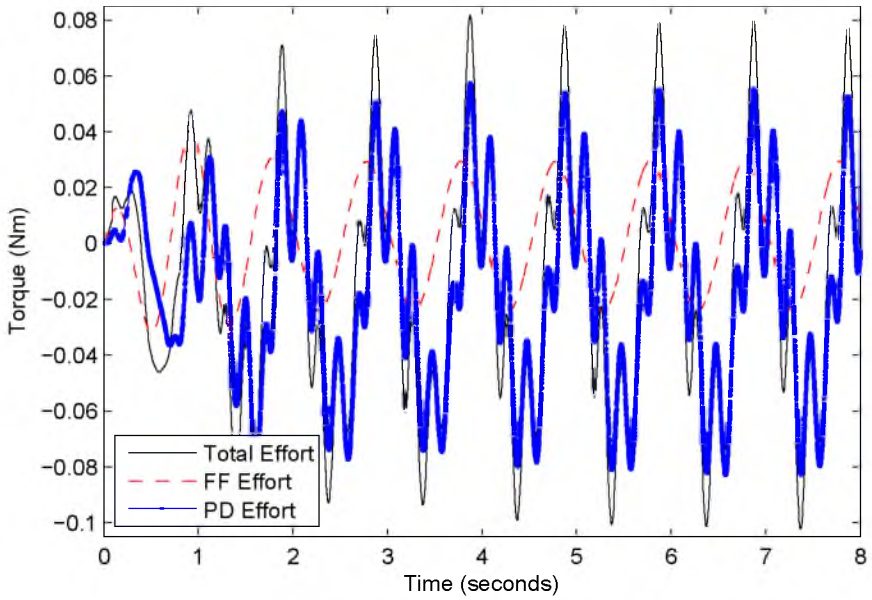

Figure 6.15. Plot of the feed-forward, PD, and total controller efforts (in motor-torque space) for the symmetric trajectory with an arm-swing frequency of 1.0 Hz and the user (1.71-m tall and 80 kg) acting passively.

trajectories seen in Chapter 2. Figure 6.11 shows data for a trial done passively with the offset trajectory, similar to the conditions in Chapter 2. It is seen that the absolute maximum torque (solid black line) is similar in scale to the torque predicted in Chapter 2. However, the feed-forward control effort is different in magnitude and offset (dashed red line). The difference is due to the different mass parameters of the subject from those used in Chapter 2. The figures all show that the PD control effort (line with points in blue) is larger than the feed-forward controller's (dashed red line). Typically, a feed-forward controller, when paired with an error-correcting PD controller, would be exptected to contribute the most to the controller output. The difference in these plots from what was expected is probably due to the approximate nature of how the inverse dynamics are implemented. The mathematical model of the human arm is used to calculated the torque required at both the shoulder and the elbow. However, only the torque required at the shoulder affects the feed-forward term. Perhaps if there were an actuator present to apply torque to the elbow, the ratio of PD to feed-forward control effort would be less than what it currently is. If the controller were purely PD, the plots would imply that if the user, while assisting, is following the desired trajectory with little error, then the total effort of the controller (i.e., the motor torque) would decrease, since PD controllers are error-based. We do not see this result most likely because the feed-forward term is "blind" to the user's efforts and

will always predict a control effort based on the inverse dynamics of the desired trajectory as if the user were passive. The PD and feed-forward terms seem to oppose each other and keep the total control effort approximately the same for both the assistive and passive user-assistance levels. This is true for both the offset and symmetric trajectories.

Next, the RMS of the motor-torque signals is considered. Figures 6.16 and 6.17 display box plots for the RMS of the motor torque for each trial, categorized by trajectory type, user-assistance level, and frequency. Again, it is observed that the symmetric trajectory's motor torque is higher than the offset trajectory's, except in the case of the assistive user level at 1.0 Hz arm-swing frequency. It is interesting to note that the reported medians for the assistive level are less than the passive level's. However, the notches, which can show a statistically significant difference in the true medians, indicate otherwise. Be that as it may, the number of data points for each box is relatively small (16), and perhaps if more trials were performed, then the notches would converge to a smaller width. Ultimately, it appears that it may not be practical to use the RMS of the motor torque signal to differentiate between whether the user is assistive or passive, at least not with the current controllers implemented. Using the RMS of the signal to confidently distinguish between the user being assistive or passive would require a large amount of time. Even if only 30 trials performed at 20 seconds each were required to show significant differences between the subject's assistance level, it would take a total of 10 minutes to come to that conclusion, which would probably not be practical. Another assumption is that the user will be able to perform the trials steadily, being able to keep their arm-swing frequency constant, which is important for converging to a single value for the RMS data. This is a hard assumption to keep in the real life, when a spinal-cord injury or stroke patient would likely not swing their arms at a steady, constant rate.

Lastly, the shoulder-angle amplitudes are examined. Figures 6.18 and 6.19 show box plots of the shoulder-angle amplitudes of the offset and symmetric trajectories, grouped by user-assistance level and arm-swing frequency. The desired arm-swing amplitude for the offset trajectory is 20 degrees and for the symmetric trajectory it is 30 degrees. For both trajectory types, there is a significant difference between the true medians in the shoulder-angle amplitudes for both arm-swing frequency and user-assistance levels. However, the statistically significant differences in the medians are only about 0.5 degrees. It is logical that the shoulder-angle amplitudes decrease for an increasing arm-swing frequency because that is something commonly seen in magnitude plots of frequency response analyses of linear dynamic systems due to the low-pass nature of inertia. The data show that when

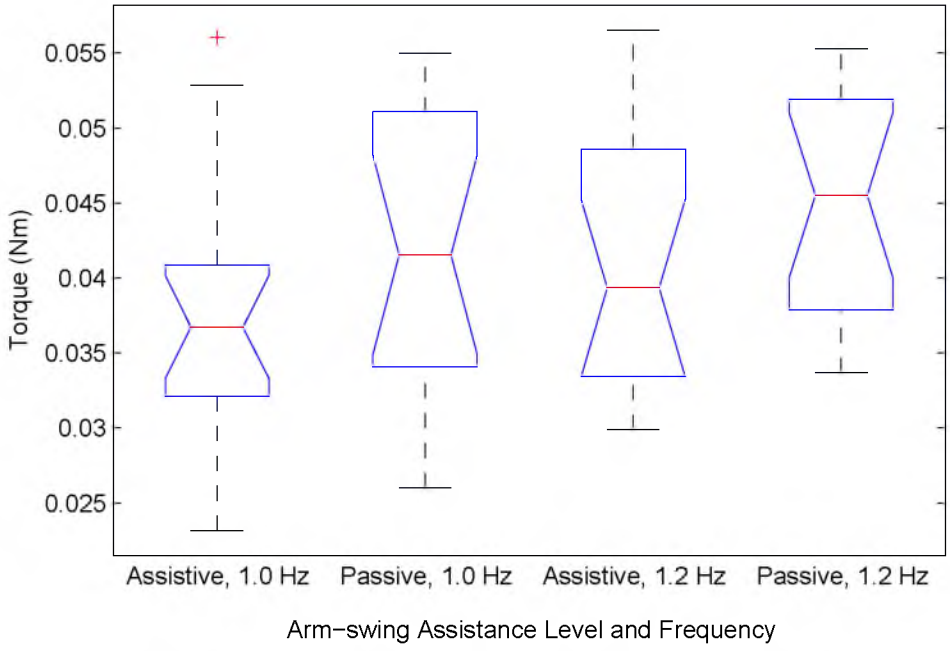

Figure 6.16. Box plots of the RMS of the motor torque signals for the offset trajectory. The data are grouped by assistance level and arm-swing frequency.

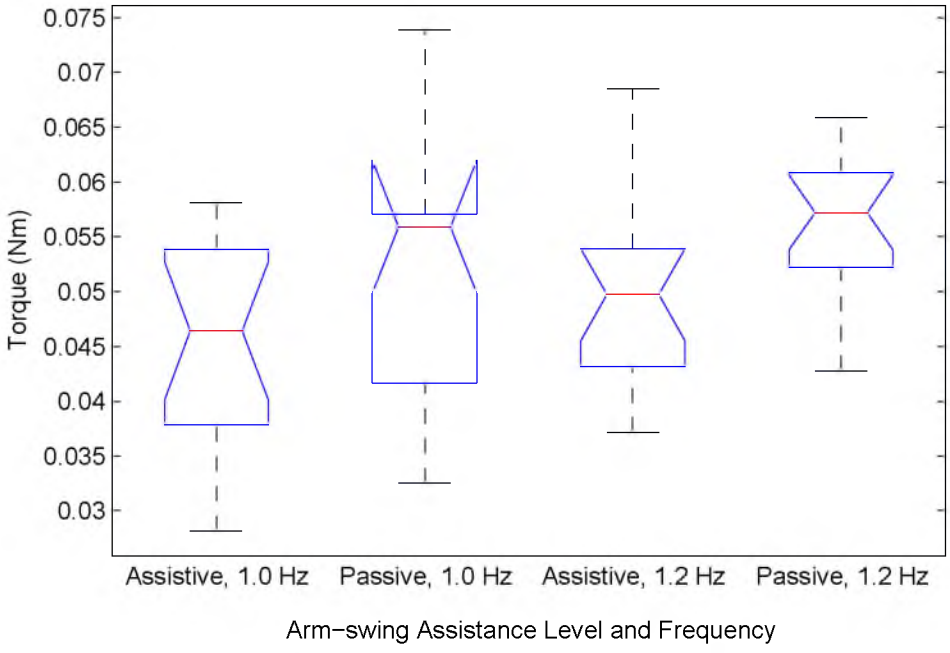

Figure 6.17. Box plots of the RMS of the motor torque signals for the symmetric trajectory. The data are grouped by assistance level and arm-swing frequency. The box for the passive, 1.0 Hz case looks unusual because the calculated notch width extends past the 75th percentile border of the box.

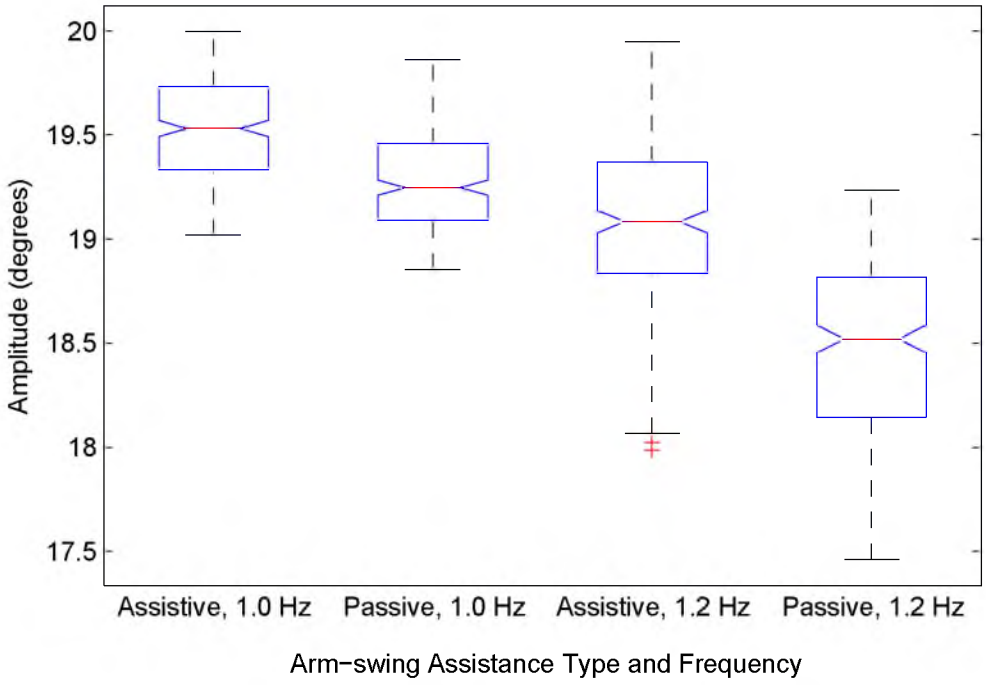

Figure 6.18. Box plots of the calculated shoulder-angle amplitudes, classified by assistance type and frequency for the offset arm trajectory.

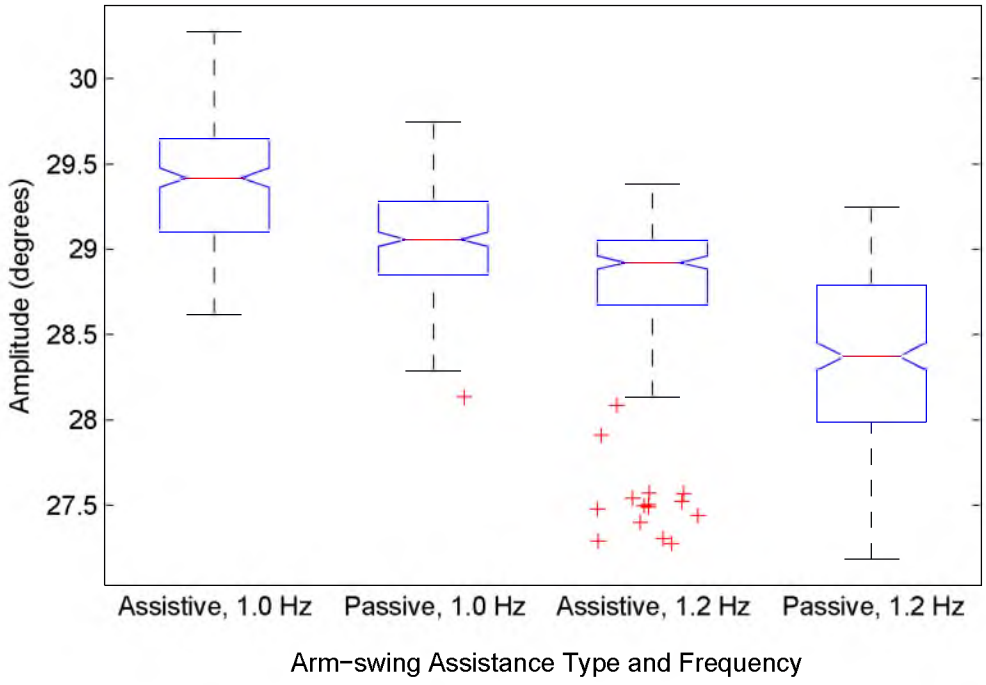

Figure 6.19. Box plots of the calculated shoulder-angle amplitudes, classified by assistance type and frequency for the symmetric arm trajectory.

a user is assisting the device, they get closer to reaching the desired amplitudes of the desired trajectory. Therefore, if it were desired to determine how much a user is assisting the UWEAR, inspecting the shoulder-angle amplitude would be a viable method, provided that the accuracy of estimating those shoulder angles is sufficient. Even if accuracy is poor, a relative change for a given user on a given day could be detected for diagnostic purposes.

6.4 Revisiting the Arm-Swing Generation Experiment

After completing the arm-swing generation experiment from the previous section, it was clear that more experiments had to be done since the feed-forward portion of the controller was incorrect to use while the user was assisting the device. This section describes a second set of experiments and the results and discussion that can be made from it.

6.4.1 Design of the Experiment

The purpose of this experiment is similar to that of the previous section; it is to evaluate the UWEAR's ability to induce arm swing in its users under the variation of different factors. What makes this experiment different is the additional factors of different controller types and different PD gains for the PD controller. The experiment seeks to find if there is a benefit—in terms of torque requirement, shoulder-angle amplitude, error tracking, or ability to diagnose a passive or active user—to using a feed-forward-plus-PD controller, rather than just a PD controller. This section's experiment also examines the effect of using high and low PD gains for the PD controller in terms of the same four quantities.

The trials for this experiment are carried out similarly to how the experiment in the previous section was done. The subjects of the test don the UWEAR and are measured in order to obtain the necessary parameters for estimating the shoulder angle from encoder measurements. The subjects stand while the UWEAR is activated and either assist the device or remain passive as arm swing of 20 degrees amplitude (from 10 degrees to -30 degrees) is induced. Motor-torque minima were again examined along with shoulder-angle amplitudes and RMS errors of the shoulder-angle trajectories once the start-up transient had decayed (the time after 5 seconds). One new feature with this experiment is that the trials lasted as long as they needed in order to capture 30 arm-flexion maxima from the user. Since the number of peaks were more important than the trial times, some trials lasted longer than others depending on the frequency being tested.

The factors that were varied from trial to trial included arm-swing frequency, the type of controller, higher and low gains for the PD controller, and the user-assistance level. Two

arm-swing frequencies of 1.0 and 0.6 Hz were tested. They represent arm-swing frequencies that are encountered at normal walking speeds, with 1.0 Hz being a realistic maximum arm-swing frequency [34], and 0.6 Hz feeling quite slow. The trial times for a frequency of 1.0 Hz lasted about 35 seconds, and trials for 0.6 Hz lasted about 55 seconds. The two different controllers that were tested were the feed-forward-plus-PD controller and the pure PD controller. The feed-forward controller in this experiment calculated torques as if the elbow were locked at 5 degrees of flexion, which is the approximate midpoint of the elbow's small range of travel during natural arm swing, and the whole upper arm acts as a single pendulum. This allows the model to calculate torques that need to be applied at only the shoulder joint, and not the shoulder and the elbow joints. High and low gains were compared only on the pure PD controller. The high gains were $k_p = 2.0\,\mathrm{N{\cdot}m/rad}$ and $k_d = 0.3\,\mathrm{N{\cdot}m/rad}$, and the low gains were $k_p = 1.0\,\mathrm{N{\cdot}m/rad}$ and $k_d = 0.15\,\mathrm{N{\cdot}m/rad}$. The high gains were tuned to be stiff yet stable to reduce the error of the PD controller; the low gains were chosen to be half of the high gains, which allow the controller to be more compliant. Both passive and assistive user-assistance levels were again considered. The feed-forward-plus-PD controller was only used in the passive case, as it was determined previously that it was illogical to use a feed-forward controller if the user is not behaving passively. The feed-forward-plus-PD controller only utilized the high PD gains.

Four healthy male subjects were tested in this experiment; their heights and weights are listed in Table 6.5. They performed 10 trials whose factors varied in a randomized order. The same hardware and software listed in the previous section was used to control the UWEAR and record data, the one exception being that the feed-forward controller was modified to simulate the arm as a single rigid body with its elbow joint locked at 5 degrees flexion.

Table 6.5. Heights and weights of the individual test participants.

Subject	Height (m)	Weight (kg)
1	1.71	80
2	1.77	65
3	1.71	70
4	1.91	94

6.4.2 Results

First, the results of the data comparing the motor torque, shoulder-angle amplitude, and RMS error for the different controller types, PD gain levels, and user-assistance levels obtained at an arm-swing frequency of 1.0 Hz will be presented, which represents a brisk walking speed. Figure 6.20 contains the box plots for these data.

The effect of the user assisting the device or remaining passive, and our ability to sense the difference between the two, will be examined first. Figure 6.20(a) contains the data for the maximum motor torques. When using the PD controller with low gains, there is no significant difference in motor torque between the passive and assistive user. When the PD controller uses the high level of PD gains, there is a significant difference in peak motor torque between the passive and assistive cases, with the passive user surprisingly requiring less peak motor torque. Figure 6.20(b) shows the data of the shoulder-angle amplitudes. The shoulder-angle amplitudes show a significant difference based on the user's assistance level at both high and low PD gains, with the user assisting the device resulting in larger shoulder-angle amplitude in both cases. Figure 6.20(c) presents the data for the RMS error of the different controllers. Neither the low gains nor high gains resulted in a significant difference between the passive and assistive cases.

Next, the effect of the level of PD gains is examined for an arm-swing frequency of 1.0 Hz. From Figure 6.20(a), when comparing the difference in the maximum motor torque due to the level of PD gains for the assistive user case, the high gains require significantly more torque than the low gains. In the passive user case, there is not a significant difference in maximum motor torque between gain levels. From Figure 6.20(b), we find that the low PD gains resulted in significantly larger shoulder-angle amplitude than the high gains in both the case of a passive user and the case of a user assisting the device (for the case of an assistive user with low PD gains, the shoulder-angle amplitudes err more since the amplitudes are larger than the desired 20 degrees). However, by looking at the box plots for the different PD gain levels, we see that the difference is subtle, which may indicate a false positive. Perhaps redoing the experiment would not show a significant difference again. If anything, in the case of a passive user, we would expect the high gains to more closely reach the desired 20 degrees than the low gains, not deviate further from it. Figure 6.20(c) shows that the RMS errors are significantly larger when using low PD gains than when using high gains, and this is true when the user is passive or assisting the device.

Next, we consider the differences between using the feed-forward-plus-PD and the pure PD controllers for an arm-swing frequency of 1.0 Hz. This will help us determine if there

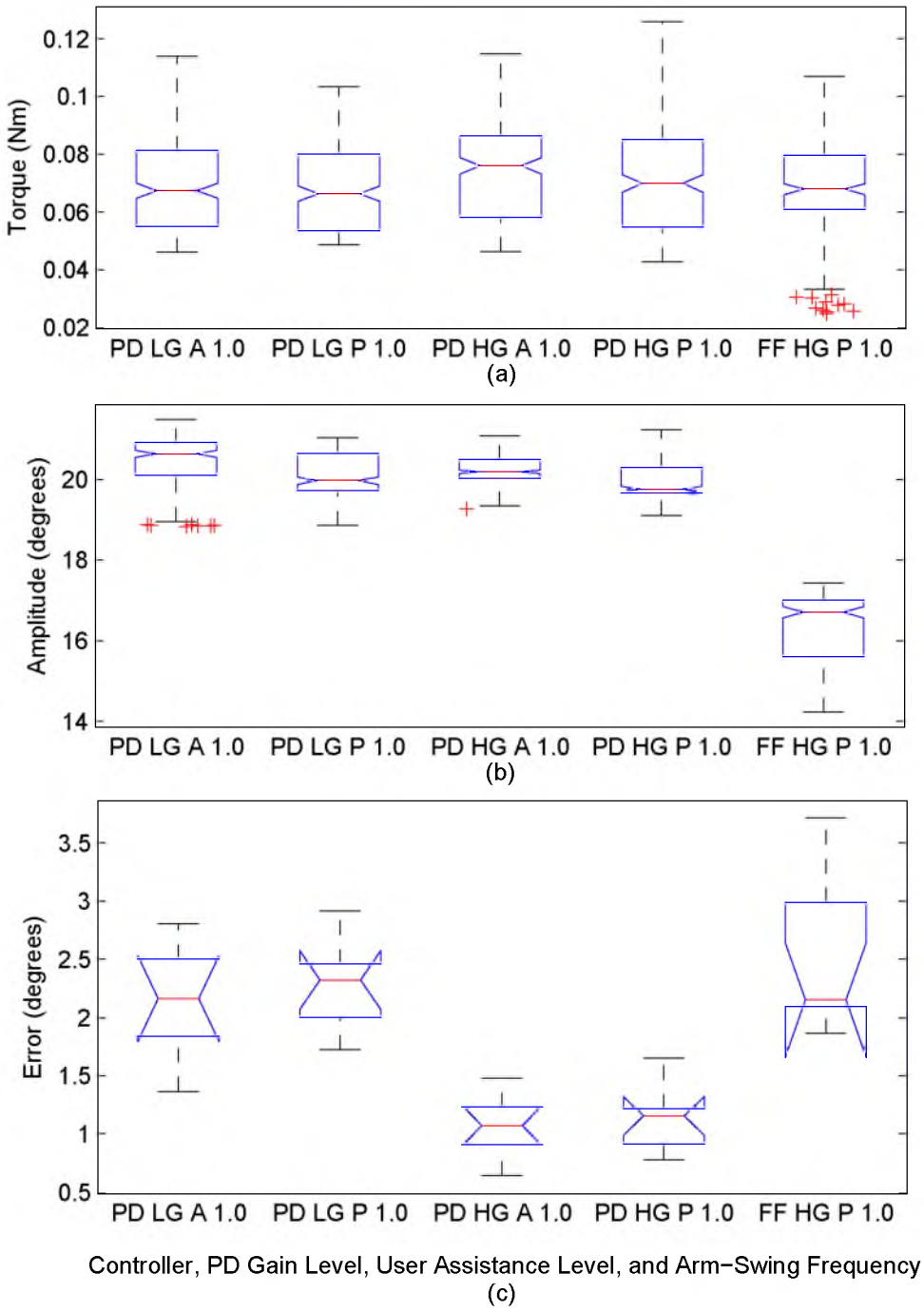

Figure 6.20. Box plots showing the results of the experiments of Section 6.4 for the trials done at 1.0 Hz arm-swing frequency. The subfigures contain the data for (a) the maximum motor torques, (b) shoulder-angle amplitude, and (c) RMS error. The individual boxes are coded by the controller type (PD = pure PD controller, FF = feed-forward-plus-PD controller), PD gain level (LG = low gains, HG = high gains), user-assistance level (A = assistive, P = passive), and arm-swing frequency (1.0 = 1.0 Hz). Note that the desired shoulder-angle amplitude is 20 degrees.

is any benefit to using one controller over the other in the case where the user is passive. From Figure 6.20(a), we find that there is no significant difference in the peak motor torques. From Figure 6.20(b), we find that there is a significant difference in the amplitude of the shoulder angle, with the pure PD controller creating a larger shoulder-angle amplitude. Finally, from Figure 6.20(c), we find that the feed-forward-plus-PD controller results in significantly higher RMS error than the pure PD controller.

Now that the results for the different factors at 1.0 Hz arm-swing frequency have been discussed, the results for the lower arm-swing frequency of 0.6 Hz will be presented. This frequency represents a slow walking speed. Figure 6.21 contains the box plots for these data.

The effect on the three metrics of the user assisting the device or remaining passive will be examined first. Figure 6.21(a) indicates that the cases where the user assists the device require significantly less peak motor torque than the cases where the user is passive, and this is true for both low and high PD gains. Figure 6.21(b) indicates that, for the PD controller with both low gains and high gains, the user assisting the device results in a shoulder-angle amplitude that is significantly larger than when the user is passive. From Figure 6.21(c), we find that there is no significant difference in RMS error between the assistive and the passive cases.

Next, the effect of the level of PD gains is examined for the arm-swing frequency of 0.6 Hz. From Figure 6.21(a), we find that the high PD gains result in significantly higher peak motor torques than the low PD gains, whether the user is passive or assisting the device. From Figure 6.21(b), we find that the high PD gains resulted in significantly larger shoulder-angle amplitude than low PD gains, and this was true whether the device was passive or assisting the device. This is different to what was seen before at higher arm-swing frequencies, but more in line with what we would expect to see. From Figure 6.21(c), we find that high PD gains resulted in significantly smaller RMS error than low PD gains, whether the user was passive or assisting the device.

Next, we consider the differences between using the feed-forward-plus-PD and the pure PD controllers at an arm-swing frequency of 0.6 Hz. As before, characterizing the differences between the two controllers will help us determine if there is any benefit to using one over the other in the case of a passive user. Figure 6.21(a) indicates that the feed-forward-plus-PD controller resulted in significantly higher peak motor torques than the pure PD controller. From Figure 6.21(b), we find that the feed-forward-plus-PD controller resulted in significantly larger shoulder-angle amplitude than the pure PD controller (i.e., significantly closer

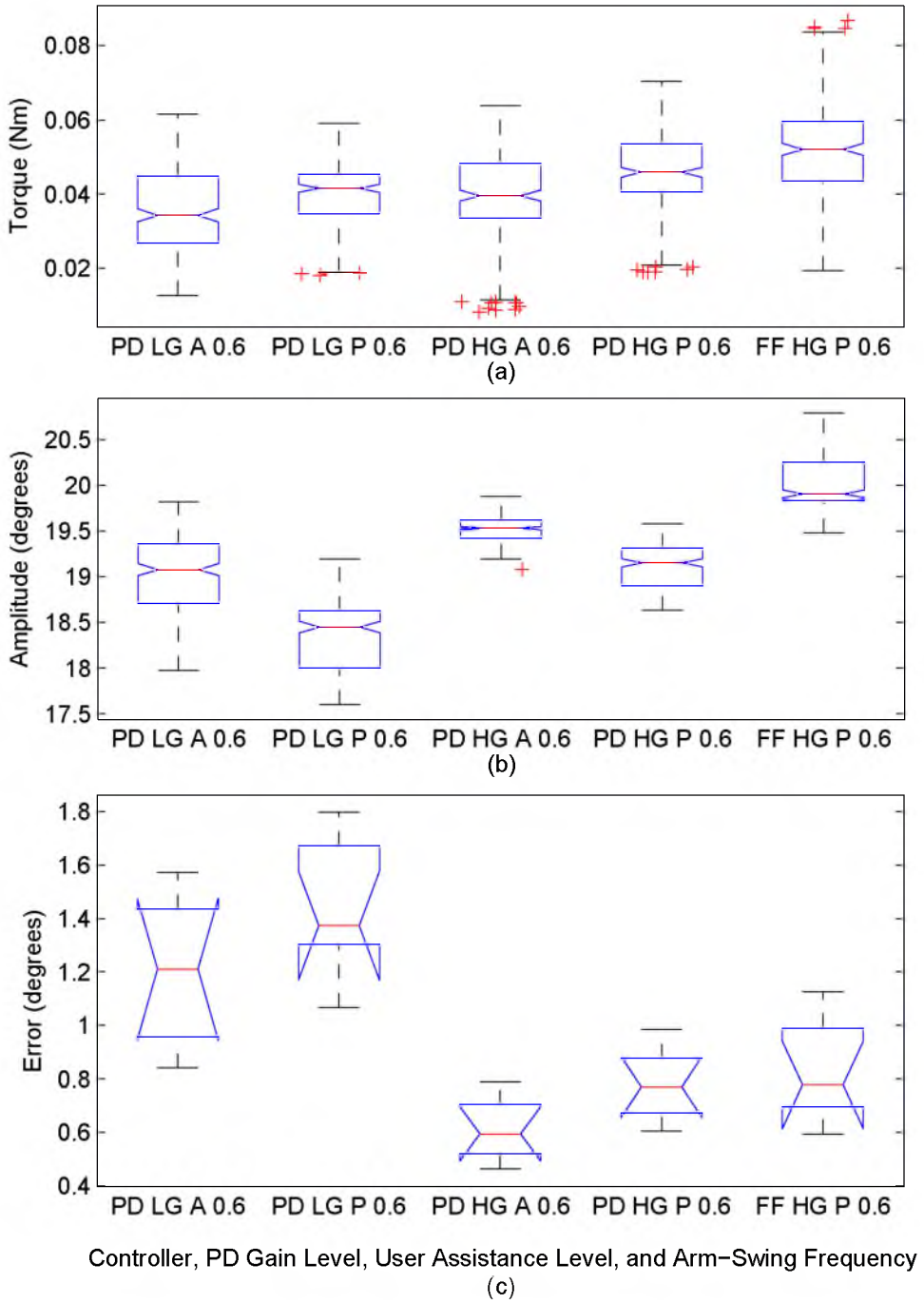

Figure 6.21. Box plots showing the results of the experiments of Section 6.4 for the trials done at 0.6 Hz arm-swing frequency. The subfigures contain the data for (a) the maximum motor torques, (b) shoulder-angle amplitude, and (c) RMS error. The individual boxes are coded by the controller type (PD = pure PD controller, FF = feed-forward-plus-PD controller), PD gain level (LG = low gains, HG = high gains), user-assistance level (A = assistive, P = passive), and arm-swing frequency (0.6 = 0.6 Hz). Note that the desired shoulder-angle amplitude is 20 degrees.

to the commanded amplitude). From Figure 6.21(c), we find that there is no significant difference in the RMS error between the two controller types.

6.4.3 Discussion

In order to interpret the results, the different controllers' performance is considered for the tracking error, shoulder-angle amplitude, and their ability to diagnose user-assistance level. The purpose of this discussion is to determine which controller is the best choice overall, at different frequencies and user-assistance levels. The discussion also contains a suggestion for the recommended controller in the case that providing more freedom to the user is more important than reaching the desired shoulder-angle amplitude.

We would like to minimize the tracking error of the UWEAR during operation for both high and low arm-swing frequencies. By examining the results of the experiment, it is found that the pure PD controller with high PD gains has the least RMS tracking error for both arm-swing frequencies and user-assistance levels. The feed-forward-plus-PD controller tracks just as well as the PD controller with high PD gains at the low arm-swing frequency, but this is only one case. The PD controller with high PD gains is the better controller when considering RMS tracking error because of the number of scenarios in which it can be utilized.

Next, it is desirable to choose the controller that minimizes the error in shoulder-angle amplitude from the desired amplitude (20 degrees). When evaluating the different controllers at the low arm-swing frequency and passive user case, the feed-forward-plus-PD controller does the best job of obtaining a shoulder-angle amplitude that matches the desired one most closely; the PD controller with high PD gains does second best. At the high arm-swing frequency, the PD controller with low PD gains creates shoulder-angle amplitudes that stray the least from the desired amplitude. When considering the different controllers in the assistive case, the PD controller with high PD gains does best in creating accurate shoulder-angle amplitudes for both low and high arm-swing frequencies. Considering all the different user-assistance levels and frequencies, the PD controller with high PD gains is the better choice in creating shoulder-angle amplitudes that most closely match the desired arm-swing amplitudes.

Next, it is advantageous to determine which controller does best in distinguishing whether the user is behaving passively or assisting the device. This discussion only involves the PD controller with high gains and low gains. At low arm-swing frequencies, both controllers can use shoulder-angle amplitude and motor torque data to distinguish the level of user assistance. At high arm-swing frequencies, the PD controller with high gains can

use both shoulder-angle amplitude and motor torque data to distinguish user assistance, whereas the PD controller with low gains can only use the shoulder-angle amplitude data. The PD controller with high PD gains appears to be the better controller for diagnosing user-assistance level because of the number of available metrics that differ significantly across both arm-swing frequencies. Interestingly, the trend for the PD controller with high gain is not consistent across arm-swing frequency for diagnosing user-assistance level. That is, at low arm-swing frequencies, the motor torques required as the user assists the device are less than when the user is passive. At high arm-swing frequencies, the relationship is reversed and the motor torques required when the user is assisting are larger than the torques required when the user is passive. The fact that the assistive level requires more motor torque at 1.0 Hz may be due to the user swinging their arm to a larger amplitude than is desired. The device has to correct the user when they are following the desired trajectory poorly. It appears that with increasing arm-swing frequency, the user may have a more difficult time following the desired trajectory when they are assisting the device, causing more error to be introduced to the controller. Since the PD controller is error based, the user following the desired trajectory inaccurately raises the torque created by the motors.

A recommendation on the controller that performs best overall can be made for future instantiations of the UWEAR. When considering the different controllers for RMS tracking error, shoulder-angle amplitude creation, and their ability to distinguish user-assistance level, the PD controller with high PD gains performs best for all arm-swing frequencies and user-assistance levels, and it is able to reliably use shoulder-angle data gathered online to determine if the user is behaving passively or actively.

It appears that the only appropriate situation for using the feed-forward-plus-PD controller would be at low frequencies while the user is essentially passive, for example, when a patient is first starting their therapy. The reason to use the feed-forward-plus-PD controller is that it seems to result in a larger shoulder-angle range of motion, at the cost of larger torque requirements. At higher frequencies, we found that the pure PD controller has less tracking error and larger shoulder-angle amplitudes than the feed-forward-plus-PD controller. This is likely the case because the mathematical model's assumption in the feed-forward-plus-PD controller that the elbow remains locked at 5 degrees flexed is no longer a valid assumption. This is thought to be the case because of the observed increased elbow motion in users at 1.0 Hz. Because of the limited cases in which the inclusion of the feed-forward controller seems beneficial, combined with the limited benefit it provides over

the pure PD controller in these cases, it may be reasonable in future work to abandon the feed-forward portion of the controller entirely.

From the results, we see that the required peak motor torques for the PD controller with low gains is significantly lower than the PD controller with high gains for the tested frequencies. We also see that there is larger shoulder-angle amplitude for the PD controller with low gains than the PD controller with high gains as the user assists the device at 1.0 Hz. We suppose that there may be more user involvement with low gains because a greater shoulder-angle amplitude is obtained with less required motor torque. More user involvement is favored in rehabilitative exercises [35]. Our experiment did not directly measure user involvement by recording muscle signals on the upper or lower limbs. Therefore, more tests, preferably with walking, are needed to directly quantify user involvement and to determine if high or low PD gains allow or prevent the user's contributions. This will help to determine if a PD controller with high gains truly is the best choice for encouraging user involvement since the PD controller with low gains, determined to be not as good as the PD controller with high gains in this experiment, can still generate arm-swing in its users.

6.5 Conclusions

The UWEAR has the potential to be a successful arm-swing device. The equations derived in Chapter 3 that are used to estimate the user's shoulder angle are fairly accurate. For the poses examined, the relative error is close to 13% in each case. Accuracy could be improved by adding another sensor and by upgrading the flexion/extension bearing to have less slop. However, if that is not practical, it should be understood that the UWEAR is not to be used as a high-accuracy positioning device in rehabilitation and that relative improvements for individual users can still be detected.

The motors operate safely and are sufficiently powerful for providing adequate torque for the examined trajectory types, user-assistance levels, and expected arm-swing frequencies. The motors could be replaced with smaller ones that provide less torque and still provide the required torques with the possible benefit of decreasing the total weight of the UWEAR.

When considering RMS tracking error, reaching the desired shoulder-angle amplitude, and the ability to diagnose user-assistance level, using a PD controller with high gains is best for the different tested frequencies and user-assistance levels. There may be scenarios where using a feed-forward-plus-PD controller is more appropriate, but because of the limited cases where it can serve better than a pure PD controller, it is likely that future work will not include the feed-forward terms. In the case that providing more freedom to the user is more

important than accurately reaching the desired shoulder-angle amplitude, the controller's PD gains can be lowered to reduce the required motor torque without the tracking errors becoming too large.

CHAPTER 7

CONCLUSIONS AND FUTURE WORK

The purpose of this thesis was to design a rehabilitative device prototype that encouraged healthy arm-swing to those who have suffered a neurological injury such as spinal-cord injury or stroke. The prototype, named UWEAR, was to be low-powered, lightweight, wearable, capable of assisting the user's arm swing in the sagittal plane, and provide unhindered kinematics in all unactuated DOF. This was accomplished by designing a device that was made of three key subassemblies: the ALICE frame, the underactuated arm-swing mechanism, and the power train. Information about the dynamics and kinematics of the human arm helped guide the design of the UWEAR. Two tests were conducted to evaluate the accuracy of the device's software that predicted the position of the user's shoulder angle and to investigate the UWEAR's ability to generate arm swing. It was found that the accuracy of the shoulder-angle prediction equations were somewhat inaccurate and that this should be remembered when using the UWEAR. The UWEAR provided sufficient motor torque for the user for both assisted and passive user-assistance levels. There was no significant difference in the torque required for the passive and assisted user-assistance levels. This was thought to be due to the conflict between the feed-forward and PD terms of the controller. However, there was a difference in shoulder-angle amplitude, and this could be used to observe how much the user was assisting the device. Upon performing more tests without the feed-forward and PD terms conflicting, it was seen that the motor torque, in addition to shoulder-angle amplitude, could be used to determine the user-assistance level provided that high PD gains were used. It was also determined that the PD controller with high gains performed best across different arm-swing frequencies and user-assistance levels in terms of RMS tracking error, shoulder-angle amplitude creation, and diagnosing user-assistance levels. The presented UWEAR prototype showed that its concept was feasible, but not yet optimal. Some suggestions are made here on how to further improve the design.

The UWEAR device allows all DOF of the glenohumeral joint to be unhindered ex-

cept for the internal/external rotation of the joint. New concepts for the underactuated arm-swing mechanism should be examined to create a prototype that truly allows all the shoulder's DOF to remain unhindered. This would primarily involve a redesign of the arm cuff.

The current UWEAR prototype is relatively heavy, weighing 26.9 lbs (12.2 kg). Its weight is not too much of a concern since the device can be used with a body-weight support system. However, making the UWEAR more lightweight could open up more rehabilitation applications and allow for exercises that do not depend on a body-weight support system. The motors, as previously mentioned, are oversized and could be replaced with smaller ones that provide enough torque with the added benefit of being more lightweight. The ALICE frame is another heavy component, and it could be replaced with a custom backpack or frame that is lighter and more comfortable to wear.

Some assumptions were made about the user's center of mass and how the mass of the UWEAR is distributed to make its impact on dynamic inertias and spatiotemporal gait parameters minimal. This was all done qualitatively. Performing a motion-capture analysis of subjects wearing the UWEAR while walking will be useful to see if those assumptions are true and if any adjustments should be made to improve the device.

The current calculations that predict the user's shoulder angle are not very accurate. Replacing the underactuated arm-swing mechanism's powered-axis bearings may improve accuracy by 1–2 degrees. Additional sensors measuring the length of the arm links should be investigated since measuring the changing arm-link length likely has more affect on predicting the shoulder-angle more accurately than correcting the bearing's slop. Potentiometers could be added to the UWEAR to measure the link length without significantly increasing the complexity of the device. Additional arm-link length detecting sensors have the added benefit of removing the human error that comes from measuring geometric parameters that are currently required for the shoulder-angle prediction equations.

Currently, the software of the UWEAR sends out a static sinusoidal trajectory for the user to follow independent of how fast the user may be walking (we did not perform any experiments with walking users). This was done partly because there was no existing research describing the arm-swing amplitude, phase, and frequency for different walking speeds. Methods should be developed to extract the user's walking speed and transform that into an appropriate and dynamically changing arm-swing signal to apply to the user's arm so that the UWEAR does not act as a metronome with which the user must keep pace.

Finally, the studies that motivated the UWEAR [6, 7] indicate that including arm

motions during gait rehabilitation will increase muscle activity in the lower limbs of the user. Tests recording the electrical signals in the user's lower and upper limbs should be performed to see if that is true for the UWEAR as well. Additionally, these tests can help determine whether high PD gains or low PD gains are best for cooperative user involvement.

REFERENCES

[1] National Spinal Cord Injury Statistical Center, "Spinal cord injury facts and figures at a glance," *J. Spinal Cord Med.*, vol. 36, no. 3, pp. 254–255, Feb. 2013.

[2] A. S. Go, D. Mozaffarian, V. L. Roger, E. J. Benjamin, J. D. Berry, W. B. Borden, D. M. Bravata, S. Dai, E. S. Ford, C. S. Fox *et al.*, "Heart disease and stroke statistics–2013 update: a report from the American Heart Association," *Circulation*, vol. 127, no. 1, pp. e6–e245, 2013.

[3] A. L. Behrman, M. G. Bowden, and P. M. Nair, "Neuroplasticity after spinal cord injury and training: an emerging paradigm shift in rehabilitation and walking recovery," *Phys. Ther.*, vol. 86, no. 10, pp. 1406–1425, Oct. 2006.

[4] A. L. Behrman and S. J. Harkema, "Locomotor training after human spinal cord injury: A series of case studies," *Phys. Ther.*, vol. 80, no. 7, pp. 688–700, 2000.

[5] D. S. Marigold and J. E. Misiaszek, "Whole body responses: neural control and implications for rehabilitation and fall prevention," *Neuroscientist*, vol. 15, no. 1, pp. 36–46, Feb. 2009.

[6] D. P. Ferris, H. J. Huang, and P.-C. Kao, "Moving the arms to activate the legs," *Exerc. Sport Sci. Rev.*, vol. 34, no. 3, pp. 113–120, 2006.

[7] F. Sylos-Labini, Y. P. Ivanenko, M. J. MacLellan, G. Cappellini, R. E. Poppele, and F. Lacquanti, "Locomotor-like leg movements evoked by rhythmic arm movements in humans," *PLoS ONE*, vol. 9, no. 3, Mar. 2014.

[8] D. de Kam, J. Duysens, and V. Dietz, "Do we need allowing arm movements for rehabilitation of gait?" in *Converging Clinical and Engineering Research on Neurorehabilitation*, J. L. Pons, D. Torricelli, and M. Pajaro, Eds. Berlin: Springer-Verlag, 2013, pp. 959–962.

[9] H. Elftman, "The function of the arms in walking," *Hum. Biol.*, vol. 11, no. 4, pp. 529–535, 1939.

[10] S. H. Collins, P. G. Adamczyk, and A. D. Kuo, "Dynamic arm swinging in human walking." *Proc. R. Soc. B.*, vol. 276, no. 1673, pp. 3679–3688, Oct. 2009.

[11] N. J. Tester, D. R. Howland, K. V. Day, S. P. Suter, A. Cantrell, and A. L. Behrman, "Device use, locomotor training, and the presence of arm swing during treadmill walking post-spinal cord injury," *Spinal Cord*, vol. 49, no. 3, pp. 451–456, Mar. 2011.

[12] R. Riener, L. Lunenburger, S. Jezernik, M. Anderschitz, G. Colombo, and V. Dietz, "Patient-cooperative strategies for robot-aided treadmill training: first experimental results," *IEEE Trans. Neural Syst. Rehabil. Eng.*, vol. 13, no. 3, pp. 380–394, Sept. 2005.

[13] J. F. Veneman, R. Kruidhof, E. E. G. Hekman, R. Ekkelenkamp, E. H. F. Van Asseldonk, and H. van der Kooij, "Design and evaluation of the LOPES exoskeleton robot for interactive gait rehabilitation," *IEEE Trans. Neural Syst. Rehabil. Eng.*, vol. 15, no. 3, pp. 379–386, Sept. 2007.

[14] Y. Stauffer, Y. Allemand, M. Bouri, J. Fournier, R. Clavel, P. Metrailler, R. Brodard, and F. Reynard, "The WalkTrainer–a new generation of walking reeducation device combining orthoses and muscle stimulation," *IEEE Trans. Neural Syst. Rehabil. Eng.*, vol. 17, no. 1, pp. 38–45, Feb. 2009.

[15] B. Novandy and J.-W. Yoon, "Development of gait rehabilitation robot driven by upper limb motion," in *Int. Conf. Control, Automation and Systems*, Seoul, Korea, October 2007, pp. 2383–2388.

[16] H. Schmidt, S. Hesse, C. Werner, and A. Bardeleben, "Upper and lower extremity robotic devices to promote motor recovery after stroke–recent developments," in *Proc. 26th Annu. Int. Conf. IEEE EMBS*, San Francisco, CA, September 2004, pp. 4825–4828.

[17] F. Struyf, J. Nijs, J.-P. Baeyens, S. Mottram, and R. Meeusen, "Scapular positioning and movement in unimpaired shoulders, shoulder impingement syndrome, and glenohumeral instability," *Scand. J. Med. Sci. Sports*, vol. 21, pp. 352–358, 2011.

[18] K. Jackson, J. Joseph, and S. Wyard, "A mathematical model of arm swing during human locomotion," *J. Biomechanics*, vol. 11, no. 6, pp. 277–289, 1978.

[19] M. Murray, S. Sepic, and E. Barnard, "Patterns of sagittal rotation of the upper limbs in walking," *Phys. Ther.*, vol. 47, no. 4, pp. 272–284, 1967.

[20] D. A. Winter, *Biomechanics and Motor Control of Human Movement.* New York: John Wiley & Sons, 1990.

[21] C. Clauser, J. McConville, and J. Young, "Weight, volume, and center of mass of segments of the human body," Aerospace Med. Res. Lab., Wright-Patterson Air Force Base, OH, Tech. Rep., 1969.

[22] R. Hinrichs, "Whole body movement: coordination of arms and legs in walking and running," in *Multiple Muscle Systems*, J. Winter and S. Woo, Eds. New York: Springer, 1990, ch. 45, pp. 694–705.

[23] V. Cimolin, M. Galli, G. Albertini, M. Crivellini, and J. Romkes, "Quantitative analysis of upper limbs during gait: a marker set protocol," *J. Appl. Biomater. Function. Mater.*, vol. 10, no. 1, pp. 49–55, 2012.

[24] A. M. Okamura, C. Richard, and M. R. Cutkosky, "Feeling is believing: using a force-feedback joystick to teach dynamic systems," *J. Eng. Educ.*, vol. 91, no. 3, pp. 345–349, July 2002.

[25] K. Bowen and M. O'Malley, "Adaptation of haptic interfaces for a LabVIEW-based system dynamics course," in *14th Symp. Haptic Interfaces for Virtual Environment and Teleoperator Systems*, Alexandria, VA, March 2006, pp. 147–152.

[26] T. H. Massie and J. K. Salisbury, "The PHANToM haptic interface: a device for probing virtual objects," *J. Dyn. Syst., Meas., Control*, vol. 55, no. 1, pp. 285–299, 1994.

[27] E. C. Metzger, "History of the development of the LINCLOE loadcarrying equipment," United States Army Natick Development Center Clothing Equipment and Materials Engineering Laboratory, Natick, MA, Tech. Rep., 1975.

[28] A. H. Slocum, *Precision Machine Design.* Englewood Cliffs, NJ: Prentice-Hall, 1992.

[29] C. Devroey, I. Jonkers, A. de Becker, G. Lenaerts, and A. Spaepen, "Evaluation of the effect of backpack load and position during standing and walking using biomechanical, physiological and subjective measures," *Ergonomics*, vol. 50, no. 5, pp. 728–742, Sept. 2007.

[30] R. Johnson, R. Pelot, J. Doan, and J. Stevenson, "The effect of a load position on biomechanical and physiological measures during a short duration march," Research and Technology Organization of NATO, Kingston, Canada, Tech. Rep., 2000.

[31] E. Harman, P. Frykman, C. Pandorf, W. Tharion, and R. Mello, "Physiological, biomechanical, and maximal performance comparisons of female soldiers carrying loads using prototype us marine corps modular lightweight load-carrying equipment (MOLLE) with interceptor body armor and us army all-purpose lightweight individual carrying equipment (ALICE) with pasgt body armor," U.S. Army Research Institute of Environmental Medicine, Natick, MA, Tech. Rep., 1999.

[32] F. Hellebrandt, E. Fries, E. Larsen, and L. Kelso, "The influence of the army pack on postural stability and stance mechanics." *Am. J. Physiol.*, vol. 140, no. 5, pp. 645–655, 1944.

[33] J. Bobet and R. Norman, "Effects of load placement on back muscle activity in load carriage," *Eur. J. Appl. Physiol.*, vol. 53, pp. 71–75, 1984.

[34] H. van Hedel, L. Tomatis, and R. Muller, "Modulation of leg muscle activity and gait kinematics by walking speed and bodyweight unloading," *Gait Posture*, vol. 24, pp. 35–45, 2006.

[35] A. Duschau-Wicke, J. von Zitzewitz, A. Caprez, L. Lunenburger, and R. Riener, "Path control: a method for patient-cooperative robot-aided gait rehabilitation," *IEEE Trans. Neural Syst. Rehabil. Eng.*, vol. 18, no. 1, pp. 38–48, Feb. 2010.